

Flower isoforms promote competitive growth in cancer

Esha Madan^{1,2}, Christopher J. Pelham^{2,3,10}, Masaki Nagane^{4,10}, Taylor M. Parker^{2,5,10}, Rita Canas-Marques¹, Kimberly Fazio⁶, Kranti Shaik⁶, Youzhong Yuan², Vanessa Henriques¹, Antonio Galzerano¹, Tadashi Yamashita⁴, Miguel Alexandre Ferreira Pinto¹, Antonio M. Palma¹, Denise Camacho¹, Ana Vieira¹, David Soldini⁷, Harikrishna Nakshatri⁵, Steven R. Post², Christa Rhiner¹, Hiroko Yamashita⁸, Davide Accardi¹, Laura A. Hansen⁶, Carlos Carvalho¹, Antonio L. Beltran¹, Periannan Kuppusamy⁹, Rajan Gogna^{1,2*} & Eduardo Moreno^{1*}

In humans, the adaptive immune system uses the exchange of information between cells to detect and eliminate foreign or damaged cells; however, the removal of unwanted cells does not always require an adaptive immune system^{1,2}. For example, cell selection in *Drosophila* uses a cell selection mechanism based on ‘fitness fingerprints’, which allow it to delay ageing³, prevent developmental malformations^{3,4} and replace old tissues during regeneration⁵. At the molecular level, these fitness fingerprints consist of combinations of Flower membrane proteins^{3,4,6}. Proteins that indicate reduced fitness are called Flower-Lose, because they are expressed in cells marked to be eliminated⁶. However, the presence of Flower-Lose isoforms at a cell’s membrane does not always lead to elimination, because if neighbouring cells have similar levels of Lose proteins, the cell will not be killed^{4,6,7}. Humans could benefit from the capability to recognize unfit cells, because accumulation of damaged but viable cells during development and ageing causes organ dysfunction and disease^{8–17}. However, in *Drosophila* this mechanism is hijacked by premalignant cells to gain a competitive growth advantage¹⁸. This would be undesirable for humans because it might make tumours more aggressive^{19–21}. It is unknown whether a similar mechanism of cell-fitness comparison is present in humans. Here we show that two human Flower isoforms (hFWE1 and hFWE3) behave as Flower-Lose proteins, whereas the other two isoforms (hFWE2 and hFWE4) behave as Flower-Win proteins. The latter give cells a competitive advantage over cells expressing Lose isoforms, but Lose-expressing cells are not eliminated if their neighbours express similar levels of Lose isoforms; these proteins therefore act as fitness fingerprints. Moreover, human cancer cells show increased Win isoform expression and proliferate in the presence of Lose-expressing stroma, which confers a competitive growth advantage on the cancer cells. Inhibition of the expression of Flower proteins reduces tumour growth and metastasis, and induces sensitivity to chemotherapy. Our results show that ancient mechanisms of cell recognition and selection are active in humans and affect oncogenic growth.

C9ORF7 (also known as *CACFD1*; referred to here as *hFWE*) encodes human Flower (hFWE) and generates four protein-coding splice variants (*hFWE1–hFWE4*) (Fig. 1a). Mining of the Encode database²² showed high levels of acetylation at the 27th lysine residue of the histone H3 protein (H3K27Ac) and hypersensitivity to DNAase-I around the +1 open reading frame (ORF) (Extended Data Fig. 1a, b), suggesting that the *hFWE* locus is transcriptionally active²³. The *hFWE* exons are conserved (Extended Data Fig. 1c), and alternative splicing produces four hFWE isoforms of transmembrane proteins,

with membrane-spanning domains as predicted (Fig. 1b). To identify potential hFWE^{Win} or hFWE^{Lose} isoforms (as observed in *Drosophila*⁶), we generated CRISPR-assisted MCF-7 *hFWE*^{KO} cells that expressed individual hFWE isoforms and used them for a co-culture protocol (Extended Data Fig. 1d). MCF-7 *hFWE*^{KO} cells lacked expression of *hFWE* mRNA (Extended Data Fig. 1e), but did not differ from wild-type cells in terms of proliferation (BrdU and MTT assays), cell-cycle, reactive oxygen species (ROS), annexin-V, and clonogenic assays (Extended Data Fig. 1f–k). Lentivirus-assisted overexpression of the four hFWE isoforms had no effect on cell proliferation, cell death, cell volume, cellular sphericity, or annexin-V staining when compared to MCF-7 *hFWE*^{KO} cells (Extended Data Figs. 1l, m, 2a–f, Supplementary Video 1). From these data, we conclude that, as in *Drosophila*^{3,6,18,24}, human cells homogeneously expressing single hFWE isoforms do not undergo apoptosis.

To identify potential hFWE^{Win} and hFWE^{Lose} isoforms, we performed live-cell imaging (Extended Data Fig. 1d), which showed that cells expressing hFWE1 or hFWE3 undergo cell death only when co-cultured with cells expressing either hFWE2 or hFWE4; cell death was accompanied by increased proliferation of cells expressing hFWE2 or hFWE4 (Fig. 1c, Extended Data Figs. 3a, b, 4a, Supplementary Videos 2–5). These findings suggest that hFWE2 and hFWE4 function as hFWE^{Win} isoforms whereas hFWE1 and hFWE3 function as hFWE^{Lose} isoforms. Furthermore, elimination of hFWE^{Lose}-expressing cells occurred through caspase-dependent apoptosis, because the addition of the caspase inhibitor Z-VAD-FMK inhibited this process and annexin-V staining (Extended Data Figs. 4b, 5a, b, 6a, Supplementary Videos 6, 7). Cells expressing individual isoforms (hFWE1–hFWE4) did not induce loss of co-cultured *hFWE*^{KO} cells, indicating that hFWE-mediated cell elimination requires cells that express both hFWE^{Win} and hFWE^{Lose} (Extended Data Fig. 6b, Supplementary Video 8). Elimination of hFWE^{Lose} cells was dependent on contact with hFWE^{Win} cells, because no apoptosis was observed during imaging of low-density-plated hFWE1–GFP⁺ and hFWE2–RFP⁺ cells (Extended Data Fig. 6c, Supplementary Video 9). We tested whether factors secreted by hFWE^{Win}-expressing cells were involved in cell elimination by transferring conditioned medium from hFWE2-expressing cells onto hFWE1-expressing cells and found that it had no significant effect on cell death (Extended Data Fig. 6d). Live-cell calcium imaging using Fluo-4AM dye showed that expression of individual hFWE isoforms in MCF-7 *hFWE*^{KO} cells had no effect on cellular calcium levels (Extended Data Fig. 7a, b), and the calcium chelator BAPTA-AM did not interfere with the elimination of hFWE^{Lose}-expressing cells (Extended Data Fig. 7c), suggesting that hFWE

¹Champalimaud Centre for the Unknown, Lisbon, Portugal. ²Department of Pathology, University of Arkansas for Medical Sciences, Little Rock, AR, USA. ³Center for Clinical Pharmacology, Washington University School of Medicine and St. Louis College of Pharmacy, St. Louis, MO, USA. ⁴Department of Biochemistry, School of Veterinary Medicine, Azabu University, Kanagawa, Japan. ⁵Department of Biochemistry and Molecular Biology, IU Simon Cancer Center, Indiana University School of Medicine, Indianapolis, IN, USA. ⁶Department of Biomedical Sciences, Creighton University, Omaha, NE, USA. ⁷Institute for Surgical Pathology, University Hospital and University of Zurich, Zurich, Switzerland. ⁸Department of Breast Surgery, Hokkaido University Hospital, Sapporo, Japan. ⁹Department of Radiology and Medicine, Norris Cotton Cancer Center, Geisel School of Medicine, Dartmouth College, Lebanon, NH, USA. ¹⁰These authors contributed equally: Christopher J. Pelham, Masaki Nagane, Taylor M. Parker. *e-mail: rajan.gogna@research.fchampalimaud.org; eduardo.moreno@research.fchampalimaud.org

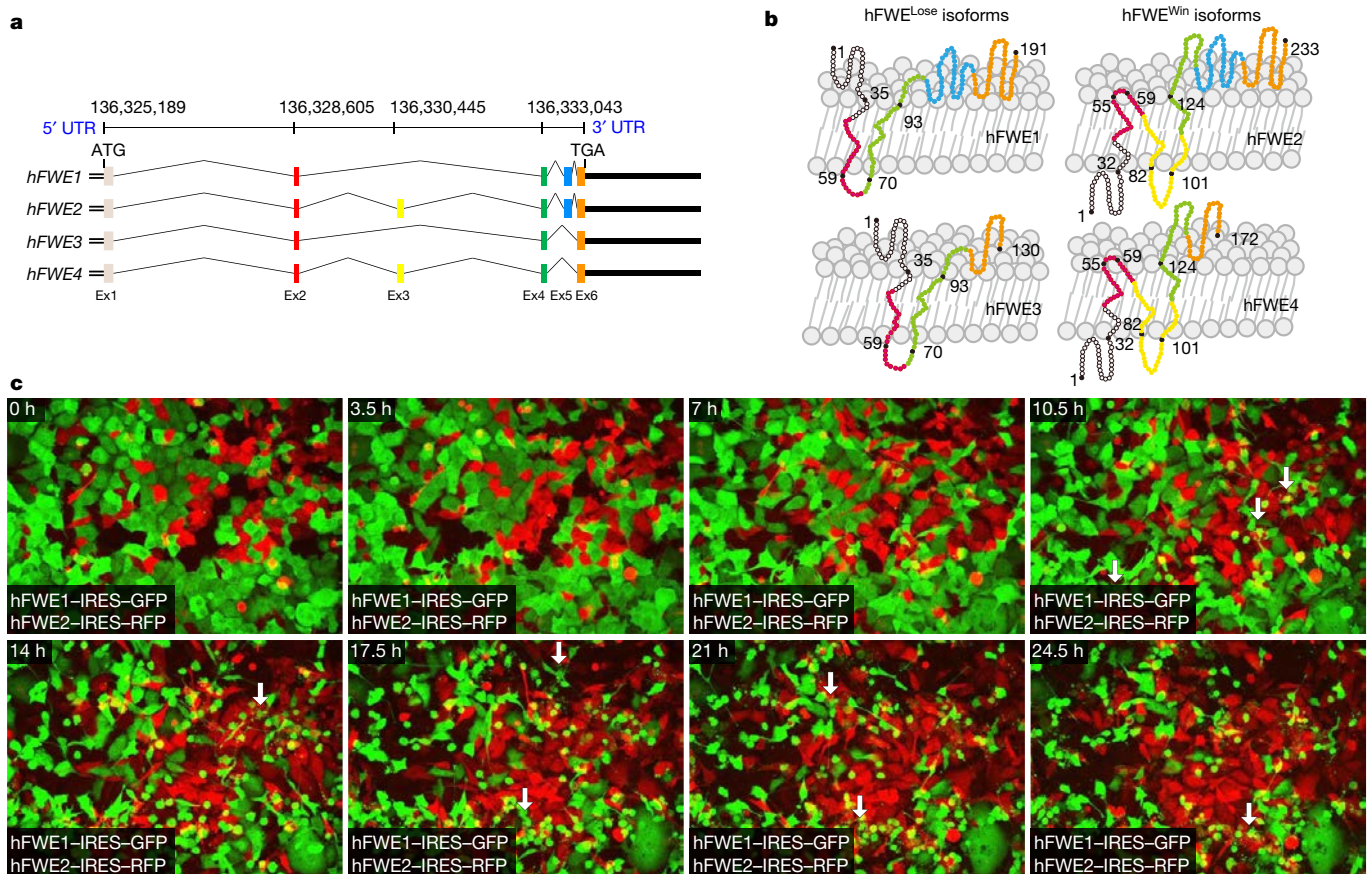


Fig. 1 | Characterization of human Flower isoforms and competition between Winner and Loser cells. **a**, A schematic representing the *hFWE* gene locus and its six exons, which alternatively splice to generate four *hFWE* isoforms (*hFWE1*–*hFWE4*). **b**, Model depicting the transmembrane structures of the four *hFWE* proteins. The colour coding of amino acid chains is complementary to the colour coding of

hFWE exons and shows the contributions and locations of the amino acid sequences coded by each exon. **c**, Live-cell imaging shows competition between *hFWE*^{KO} MCF-7 cells expressing *hFWE1*–IRES–GFP (green) and *hFWE2*–IRES–RFP (red) isoforms; cells carrying the *hFWE1* isoform are eliminated. $n = 3$ biologically independent experiments with similar results.

isoforms do not function as calcium transporters^{25–27} and their function is calcium-independent. We conclude that human Flower proteins work as canonical fitness fingerprints.

To study the role of Flower proteins in human cancer, we used quantitative PCR (qPCR) to measure the expression of *hFWE* isoforms in laser-captured formalin-fixed paraffin-embedded (FFPE) samples of cancerous and adjacent stromal tissue from individuals with malignant tumours (25 breast, 21 colon), benign tumours (10 breast, 10 colon), and normal tissue (10 breast, 10 colon, from matched patients; Fig. 2a). All *hFWE* isoforms showed poor expression in normal tissue. The tumour tissue showed increased expression of *hFWE*^{Win} isoforms, and stromal tissue showed significant upregulation of *hFWE*^{Lose} isoforms (more in malignant tumours than in benign tumours and their stroma; Fig. 2a). Sequential laser capture of breast and colon stromal tissue showed a significant increase in expression of *hFWE*^{Lose} isoforms in the first 400 μm from the edge of the tumour tissue (Extended Data Fig. 7d), where genes involved in the regulation of apoptosis were concurrently upregulated (Extended Data Fig. 7e). Fluorescence in situ hybridization (FISH) showed increased expression of *hFWE*^{Win} isoforms exclusively in breast cancer cells (Extended Data Fig. 7f); further qPCR showed that, unlike tumour epithelial cells, normal epithelial cells do not exhibit high *hFWE*^{Win} expression (Extended Data Fig. 7g). MCF-7 *hFWE*^{KO} cells expressing *hFWE2* induced apoptosis of co-cultured primary epithelial cells or fibroblasts (isolated from normal breast tissue; Extended Data Fig. 8a).

We generated two anti-*hFWE* antibodies (one against the N terminus that is common to all four isoforms, and the other specific to the *hFWE*^{Win} isoforms (encoded by exon 3)). We used

immunohistochemistry to validate the antibody specificity in sections of *hFWE*^{KO} cells overexpressing *hFWE1*, *hFWE2*, *hFWE3* or *hFWE4* (Extended Data Figs. 8b, 9a). Immunostaining with anti-*hFWE*^{Win} and anti-*hFWE*-N-term antibodies produced positive membrane staining in breast cancer cells (Extended Data Fig. 9b). Immunohistochemistry with the anti-*hFWE*^{Win} antibody showed that *hFWE*^{Win} was expressed exclusively in breast, colon, and squamous cell carcinoma (SCC) cancers (Fig. 2b, Extended Data Figs. 7h, 9c). Immunohistochemistry of the same breast, colon, and SCC cancers with anti-*hFWE*-N-term antibodies—which recognize both *hFWE*^{Win} and *hFWE*^{Lose} isoforms—showed staining of both cancer and stromal cells (Fig. 2b, Extended Data Figs. 7h, 9c). Both antibodies showed poor staining in normal tissue (Extended Data Fig. 9c). Our main observations from this analysis were that both types of *hFWE* isoform tend to be low in healthy tissue, *hFWE*^{Win} isoforms are upregulated in cancer tissue (more in malignant than in benign cancers), and levels of *hFWE*^{Lose} isoforms are unusually high in the cancer-adjacent stroma.

These results suggested that tumour cells exhibit high *hFWE*^{Win} expression and tend to grow in areas of stroma with high *hFWE*^{Lose} expression. To investigate whether overexpression of *hFWE*^{Lose} in host tissue and *hFWE*^{Win} in the tumour might result in aggressive tumour growth, we generated *Fwe*^{KO} mice²⁶ bearing orthotopic breast tumours derived from MCF-7 cells. Individual *hFWE* isoforms were overexpressed in the mammary tissue of *Fwe*^{KO} mice to study the effects of host cells, and *hFWE*^{KO} MCF-7 cells overexpressing GFP-tagged individual *hFWE* isoforms were used to generate the tumours (Fig. 3a). When we analysed all possible combinations, we found that MCF-7 *hFWE*^{KO} cells expressing *hFWE2*–GFP or *hFWE4*–GFP generated

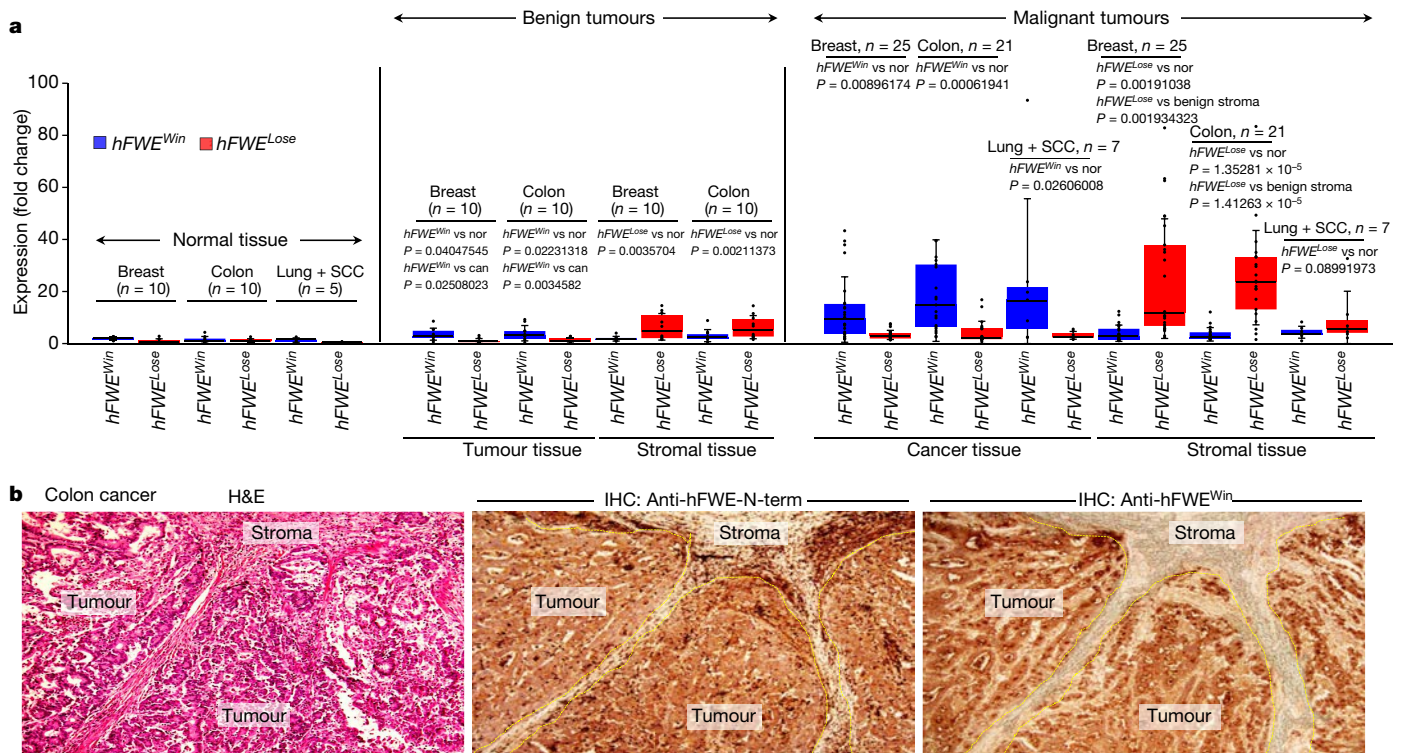


Fig. 2 | Flower isoforms and human cancer. **a**, Expression of hFWE^{Win} and hFWE^{Lose} mRNA is observed in benign and malignant tumours, their respective stroma (from same samples) and healthy tissue (laser microdissected, FFPE samples). Poor expression was observed in healthy tissue; hFWE^{Win} isoforms were upregulated in benign tumour tissue; and hFWE^{Lose} isoforms were upregulated in stromal tissue. In malignant tumours, hFWE^{Win} isoforms were significantly upregulated in cancer tissue and hFWE^{Lose} isoforms were significantly upregulated in stromal tissue. hFWE^{Win} expression ratio for normal:benign tumour:malignant tumour, 1:2.328:11.369. hFWE^{Lose} expression ratio for normal:benign stroma:malignant stroma, 1:6.513:24.694. By binary logistic regression analysis, hFWE^{Win} in cancer (with $P = 0.006$) and hFWE^{Lose} in stroma

(with $P = 0.015$) together have predictive capacity for malignant tumours of 86.3%. n represents the number of biologically independent experiments and fold change is calculated against the expression of hFWE^{Win} isoforms in normal breast tissue. Box plots show median, first and third quartiles, positive and negative error values (s.d.). All statistically significant P values are shown (two-tailed t -test). Nor, normal tissue; can, cancer tissue. **b**, Left, haematoxylin and eosin (H&E) stained colon cancer and stromal samples. Right, immunostaining of colon cancer samples shows the abundance of hFWE^{Win} isoforms. Middle, staining with anti-hFWE-N-term antibody shows staining in both tumour and stroma. This experiment was repeated independently three times with similar results.

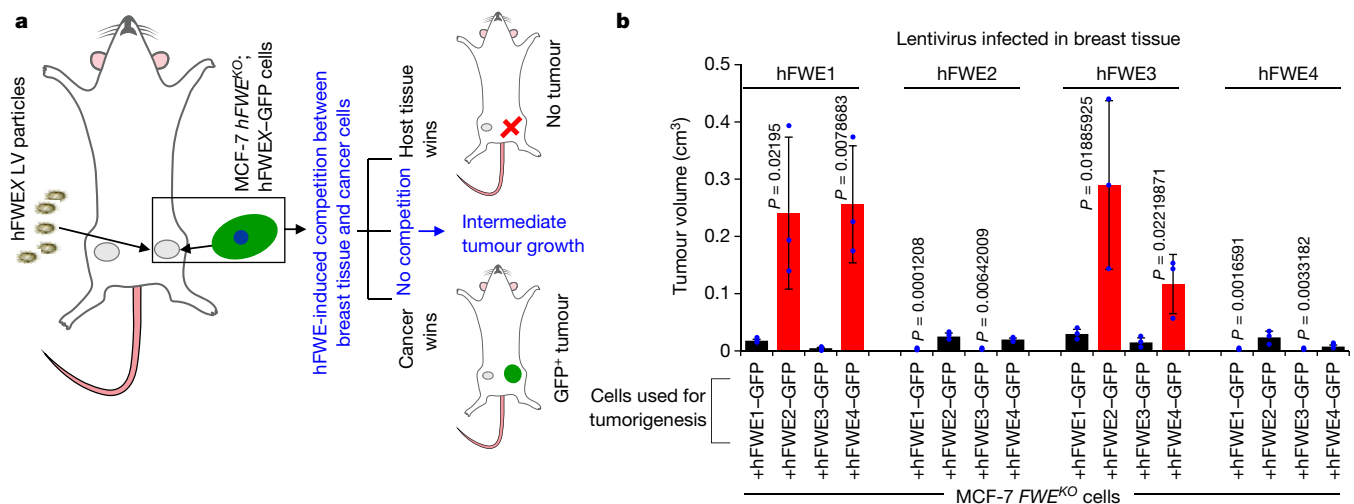


Fig. 3 | Lose isoform in stroma and Win isoform in tumour cooperate to induce aggressive cancer growth. **a**, Schematic of mouse model used to study competition between injected hFWE^{Win}- or hFWE^{Lose}-expressing cancer cells and hFWE^{Win}- or hFWE^{Lose}-expressing host tissue. hFWEX represents any one of hFWE1–hFWE4. LV, lentivirus. **b**, Tumour volumes were measured and analysed for each of the 16 combinations of hFWEX-IRES-GFP expression in MCF-7 hFWE^{KO} xenografted cells and hFWE

isoform expression within *Fwe*^{KO} mouse mammary tissue (28-day study). Reduced tumour growth was observed when mammary tissue expressed hFWE^{Win} isoforms and cancer cells expressed hFWE^{Lose} isoforms. Increased tumour growth was observed when mammary tissue expressed hFWE^{Lose} isoforms and cancer cells expressed hFWE^{Win} isoforms. $n = 3$, all statistically significant P values shown, two-tailed t -test, mean \pm s.d.

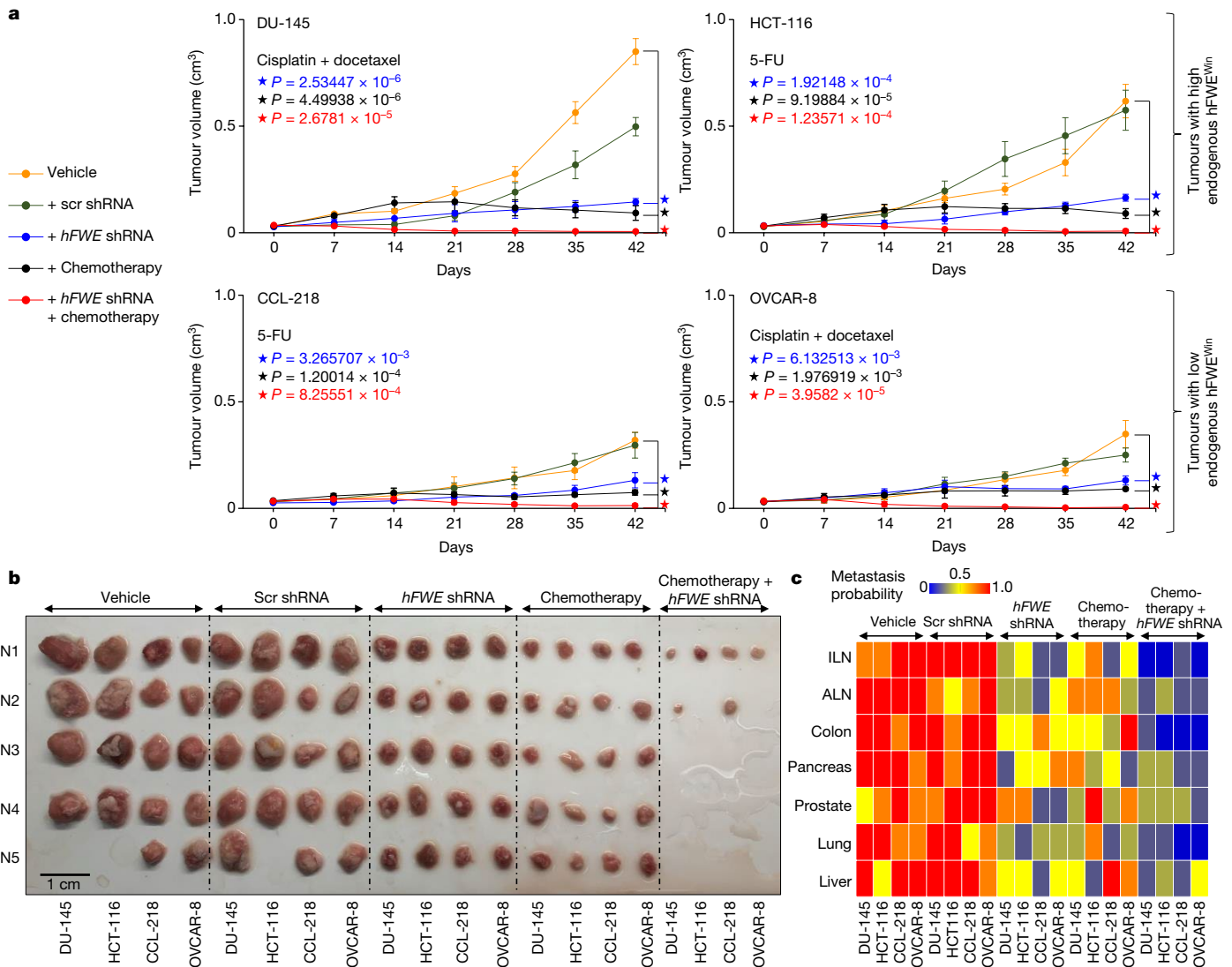


Fig. 4 | *hFWE* knockdown inhibits tumorigenicity and improves chemotherapy efficiency. **a**, **b**, The effect of shRNA-mediated *hFWE* knockdown on the tumour growth potential of DU-145 (prostate), HCT-116 (colon), CCL-218 (colon) and OVCAR-8 (ovarian) cell lines was tested. Orange, control vehicle-treated tumours; green, negative control non-specific scrambled (Scr) shRNA-treated tumours; blue, tumours treated with a cocktail of anti-*hFWE* shRNA, resulting in a significant reduction in tumour volume; black, cisplatin + docetaxel for prostate (DU-145) and ovarian (OVCAR-8) lines and 5-FU for colon cancer lines (HCT-116 and CCL-218); red, a combination of *hFWE* knockdown with

chemotherapy abolishes tumour burden in several cases and overall significantly reduces tumour growth. $n = 5$ biologically independent experiments, P values shown, mean \pm s.d., one-tailed t -test. **c**, The effect of treatment with vehicle, scrambled shRNA, *hFWE* shRNA, chemotherapy, and a combination of *hFWE* shRNA and chemotherapy on metastasis. Heat map scale indicates the probability of metastasis, which is significantly reduced by treatment with *hFWE* shRNA or a combination of *hFWE* shRNA and chemotherapy (compare groups 1 and 2 with groups 3, 4 and 5; $n = 5$ each group).

aggressive tumours when implanted into mammary tissue expressing *hFWE1* or *hFWE3* (Fig. 3b, Extended Data Fig. 9d). The results suggest that interactions between expression of *hFWE*^{Win} isoforms in tumours and *hFWE*^{Lose} isoforms in the stroma are important for tumour growth.

We investigated the role of host tissue *hFWE* isoforms by using *hFWE2*-overexpressing *hFWE*^{KO} HCT-116 and MCF-7 cells to generate tumours in *Fwe*^{WT} and *Fwe*^{KO} mice. Both HCT-116 *hFWE2*⁺ and MCF-7 *hFWE2*⁺ tumours were larger with higher incidences of metastasis in *Fwe*^{WT} mice than in *Fwe*^{KO} mice (Extended Data Fig. 9e–g). The expression of *hFWE*^{Lose} isoforms was upregulated in wild-type MCF-7 cells when they were co-cultured with *hFWE2*-expressing *hFWE*^{KO} MCF-7 cells (Extended Data Fig. 10a, b). Similarly, expression of *hFWE*^{Lose} isoforms was increased in tumour-adjacent tissue from *Fwe*^{WT} mice after implantation of *hFWE2*-expressing MCF-7 tumours when compared with before (Extended Data Fig. 10c). From these experiments, we conclude that the expression of Win isoforms in the tumour is sufficient to induce increased expression of Lose isoforms non-autonomously in the

surrounding cells. These data show that stromal Lose and tumoral Win isoforms cooperate to promote aggressive cancer growth.

Next, we tested whether inhibition of Flower could provide anti-cancer benefits. Amongst ectopic tumours derived from *hFWE*^{WT} and *hFWE*^{KO} HCT-116 cells, those derived from *hFWE*^{WT} cells were larger (Extended Data Fig. 10d, e). Knockdown of *hFWE* expression by short hairpin RNA (shRNA) in *hFWE*^{WT} HCT-116 cells before xenografting (Extended Data Fig. 10g, h) reduced both tumour volume and probability of metastasis (Extended Data Fig. 10d–f). The growth (Extended Data Fig. 10d, e) and metastatic potential (Extended Data Fig. 10f) of HCT-116 tumours treated with shRNA targeting *hFWE* was rescued by ectopic expression of codon-optimized *hFWE2* cDNA (which is unaffected by anti-*hFWE* shRNA) (Extended Data Fig. 10h). In a gain-of-function experiment, we overexpressed *hFWE2* in CCL-218 (colon cancer) cells, which express low levels of *hFWE*^{Win} isoforms; this resulted in a nearly threefold increase in their tumour growth potential (Extended Data Fig. 10i, j).

We screened a panel of 18 metastatic cell lines of multiple origins (breast, colon, prostate, pancreatic, and ovarian) for $hFWE^{Win}$ expression (Extended Data Fig. 10j). Cells with higher (HCT-116 colon and DU-145 prostate) or lower (CCL-218 colon and OVCAR-8 ovarian) expression of $hFWE^{Win}$ were selected, and their tumorigenic potential was observed. We tested the therapeutic potential of $hFWE$ gene knockdown (Extended Data Fig. 10g) in combination with standard-of-care chemotherapy against the tumorigenic potential of these cancer cell lines. DU-145 and HCT-116 cells had significantly higher tumorigenic potential and generated larger tumours than CCL-218 and OVCAR-8 cells (Fig. 4a, b). $hFWE$ knockdown significantly reduced tumour volumes (Fig. 4a, b). Control xenografts and those treated with scrambled shRNA generated much larger tumours than xenografts treated with anti- $hFWE$ shRNA or chemotherapy (fluorouracil (5-FU) for colon cancer²⁸, or cisplatin and docetaxel for prostate²⁹ and ovarian³⁰ cancer). Treatment with a combination of anti- $hFWE$ shRNA and chemotherapy further reduced, and in some cases completely eliminated, tumorigenesis (Fig. 4a, b). Control experiments demonstrated the efficiency of $hFWE$ shRNA in all tumours (Extended Data Fig. 10k). Metastatic probability was reduced markedly upon $hFWE$ knockdown and even further by combined treatment with chemotherapy (Fig. 4c). Thus, we conclude that human $hFWE$ proteins can have a powerful effect on tumorigenicity and propose that therapies targeting these proteins have the potential to impair cancer growth and metastasis.

We have shown that the human Flower protein code mediates competitive interactions that depend on cell contact and caspase-dependent apoptosis but not on calcium transport. Homogeneous expression of any of the four Flower proteins does not trigger cell elimination or affect cell fitness in terms of proliferation, survival, or clonogenicity. Cell elimination requires different levels of Win and Lose isoforms in neighbouring cells, demonstrating that relative levels of these proteins are more important than absolute levels for cell selection. In addition, we find that human tumours use cell fitness markers to gain a competitive advantage over neighbouring cells. This work represents a conceptual advance in understanding the role of cell fitness comparisons in the progression of human cancer. It describes a concrete molecular mechanism that regulates oncogenic growth and metastasis via the Flower fitness comparison system. This appears to be a striking general feature of solid tumours and an unrecognized prerequisite for tumour growth. Notably, we also show that inhibition of cell competition can be combined with standard-of-care chemotherapy to further prevent tumour growth and metastasis of colon, ovarian and prostate cancers.

Online content

Any methods, additional references, Nature Research reporting summaries, source data, extended data, supplementary information, acknowledgements, peer review information; details of author contributions and competing interests; and statements of data and code availability are available at <https://doi.org/10.1038/s41586-019-1429-3>.

Received: 4 May 2016; Accepted: 26 June 2019;

Published online 24 July 2019.

1. Medzhitov, R. & Janeway, C. A. Jr Decoding the patterns of self and nonself by the innate immune system. *Science* **296**, 298–300 (2002).
2. Vivier, E. et al. Innate or adaptive immunity? The example of natural killer cells. *Science* **331**, 44–49 (2011).
3. Merino, M. M. et al. Elimination of unfit cells maintains tissue health and prolongs lifespan. *Cell* **160**, 461–476 (2015).

4. Merino, M. M., Rhiner, C., Portela, M. & Moreno, E. “Fitness fingerprints” mediate physiological culling of unwanted neurons in *Drosophila*. *Curr. Biol.* **23**, 1300–1309 (2013).
5. Moreno, E., Fernandez-Marrero, Y., Meyer, P. & Rhiner, C. Brain regeneration in *Drosophila* involves comparison of neuronal fitness. *Curr. Biol.* **25**, 955–963 (2015).
6. Rhiner, C. et al. Flower forms an extracellular code that reveals the fitness of a cell to its neighbors in *Drosophila*. *Dev. Cell* **18**, 985–998 (2010).
7. Merino, M. M., Levayer, R. & Moreno, E. Survival of the fittest: essential roles of cell competition in development, aging, and cancer. *Trends Cell Biol.* **26**, 776–788 (2016).
8. Gogna, R., Shee, K. & Moreno, E. Cell competition during growth and regeneration. *Annu. Rev. Genet.* **49**, 697–718 (2015).
9. Di Gregorio, A., Bowling, S. & Rodriguez, T. A. Cell competition and its role in the regulation of cell fitness from development to cancer. *Dev. Cell* **38**, 621–634 (2016).
10. Greaves, M. & Maley, C. C. Clonal evolution in cancer. *Nature* **481**, 306–313 (2012).
11. Jacobs, K. B. et al. Detectable clonal mosaicism and its relationship to aging and cancer. *Nat. Genet.* **44**, 651–658 (2012).
12. Kennedy, S. R., Loeb, L. A. & Herr, A. J. Somatic mutations in aging, cancer and neurodegeneration. *Mech. Ageing Dev.* **133**, 118–126 (2012).
13. Laurie, C. C. et al. Detectable clonal mosaicism from birth to old age and its relationship to cancer. *Nat. Genet.* **44**, 642–650 (2012).
14. López-Otín, C., Blasco, M. A., Partridge, L., Serrano, M. & Kroemer, G. The hallmarks of aging. *Cell* **153**, 1194–1217 (2013).
15. Vanneste, E. et al. Chromosome instability is common in human cleavage-stage embryos. *Nat. Med.* **15**, 577–583 (2009).
16. Vijg, J. Somatic mutations, genome mosaicism, cancer and aging. *Curr. Opin. Genet. Dev.* **26**, 141–149 (2014).
17. Neves, J., Demaria, M., Campisi, J. & Jasper, H. Of flies, mice, and men: evolutionarily conserved tissue damage responses and aging. *Dev. Cell* **32**, 9–18 (2015).
18. Levayer, R., Hauert, B. & Moreno, E. Cell mixing induced by myc is required for competitive tissue invasion and destruction. *Nature* **524**, 476–480 (2015).
19. Klein, C. A. Selection and adaptation during metastatic cancer progression. *Nature* **501**, 365–372 (2013).
20. Maruyama, T. & Fujita, Y. Cell competition in mammals—novel homeostatic machinery for embryonic development and cancer prevention. *Curr. Opin. Cell Biol.* **48**, 106–112 (2017).
21. Moreno, E. Is cell competition relevant to cancer? *Nat. Rev. Cancer* **8**, 141–147 (2008).
22. ENCODE Project Consortium. An integrated encyclopedia of DNA elements in the human genome. *Nature* **489**, 57–74 (2012).
23. Ji, X. et al. Chromatin proteomic profiling reveals novel proteins associated with histone-marked genomic regions. *Proc. Natl Acad. Sci. USA* **112**, 3841–3846 (2015).
24. Moreno, E. & Rhiner, C. Darwin’s multicellularity: from neurotrophic theories and cell competition to fitness fingerprints. *Curr. Opin. Cell Biol.* **31**, 16–22 (2014).
25. Chang, H. F. et al. Cytotoxic granule endocytosis depends on the Flower protein. *J. Cell Biol.* **217**, 667–683 (2018).
26. Petrova, E., López-Gay, J. M., Rhiner, C. & Moreno, E. Flower-deficient mice have reduced susceptibility to skin papilloma formation. *Dis. Model. Mech.* **5**, 553–561 (2012).
27. Xue, L. et al. Voltage-dependent calcium channels at the plasma membrane, but not vesicular channels, couple exocytosis to endocytosis. *Cell Rep.* **1**, 632–638 (2012).
28. Zhang, P. et al. Curcumin synergizes with 5-fluorouracil by impairing AMPK/ULK1-dependent autophagy, AKT activity and enhancing apoptosis in colon cancer cells with tumor growth inhibition in xenograft mice. *J. Exp. Clin. Cancer Res.* **36**, 190 (2017).
29. Davies, A. H., Wang, Y. & Zoubeidi, A. Patient-derived xenografts: A platform for accelerating translational research in prostate cancer. *Mol. Cell. Endocrinol.* **462**, 17–24 (2018).
30. Chang, C. E. et al. Novel application of pluronic lecithin organogels (PLOs) for local delivery of synergistic combination of docetaxel and cisplatin to improve therapeutic efficacy against ovarian cancer. *Drug Deliv.* **25**, 632–643 (2018).

Publisher’s note: Springer Nature remains neutral with regard to jurisdictional claims in published maps and institutional affiliations.

© The Author(s), under exclusive licence to Springer Nature Limited 2019

METHODS

Bio-informatics analysis. Encode data for the *CACFD1* (*hFWE*) gene were collected systematically from the UCSC Genome Browser. The trans-membrane structures for human *hFWE* isoforms were predicted using Predictprotein 2013 software from the Technical University of Munich.

Established cell lines and culture conditions. A2780-CR, A2780-CS, CCL-218, DU-145, HCC-1954, HCT-116, MCF-7, MCF 10A, MD-4, MD-7, MDA-MB-231, MDA-MB-468, PC-3, SK-BR-3, TR-127, TR-182 and ZR-75 cells were procured with certificates of authentication from the American Type Culture Collection (ATCC). HEK293 cells were procured from Cell Biolabs. OVCAR-4 and OVCAR-8 cells were kindly provided by S. Karuppaiyah (Ohio State University). In brief, all cell lines were cultured as suggested by the ATCC in Dulbecco's modified Eagle's medium (DMEM) or RPMI 1640 (Corning) supplemented with 10% (v/v) heat-inactivated fetal bovine serum (FBS) (Gibco) and 1% (v/v) penicillin/streptomycin (Thermo Fisher Scientific) and incubated at 37 °C in a humidified atmosphere of 95% air and 5% CO₂. Cell lines were tested for mycoplasma contamination.

Transfections and preparation of lentiviral particles. All transfections were performed using Lipofectamine 3000 (Thermo Fisher Scientific). Lentiviral particles encoding Cas9 + *hFWE* single guide RNA (sgRNA), *hFWE* shRNA, and cDNA for *hFWE1*–*hFWE4* were generated using HEK293T cells and their respective packaging. The viral particles were concentrated by centrifuging the supernatant at 22,000 r.p.m. for 2 h at 20 °C. The pellet was re-suspended in 200 μ l 1 \times HBSS, purified by layering the 200 μ l of viral preparation on 1.5 ml of 20% sucrose (in HBSS) and centrifugation at 22,000 r.p.m. for 2 h at 20 °C, and then the pellet was re-suspended in 100 μ l 1 \times HBSS. The titre of lentiviral particles was determined using a p24 ELISA kit (Cell Biolabs); 10⁹ TU ml⁻¹ was used for cell culture experiments, and 10¹¹ TU ml⁻¹ was used for *in vivo* infections. For infection of target cells, lentiviral particles were diluted in culture medium containing 5 μ g ml⁻¹ polybrene (Thermo Fisher Scientific).

Generation of MCF-7 and HCT-116 *hFWE*^{KO} cells. Stable knockout of *hFWE* was performed using lentiCRISPR V2 vector (Addgene) expressing both Cas9 and sgRNA targeting the *hFWE* gene loci. Cloning of sgRNA targeting *hFWE* gene loci was performed as described previously^{31,32}. Lentiviral particles were generated by transfection of HEK293T cells with lentiCRISPRs, psPAX2, and pMD2.G plasmids (Addgene) and the virus was collected 48 h later^{31,32}. MCF-7 and HCT-116 cells were infected with lentiviral particles, and 48 h later the medium was replaced with culture medium containing 2 μ g ml⁻¹ puromycin (Thermo Fisher Scientific). After 2 weeks of puromycin selection, single-cell colonies were isolated via ring cloning. DNA from each colony was extracted using QuickExtract (Epicentre). To confirm that an indel was present at both alleles, the region, including the target site, was amplified using PCR. The PCR products were ligated into pBlueScript (Addgene) for cloning and sequencing. Oligos for creating CRISPRs: *CACFD1*-csp1a: CACCGCATGACGTGGTGGTACCGC, *CACFD1*-csp1b: AAACGCGGTACCACACGTCATGC, *CACFD1*-csp2a: caccTTCAAGCTTGCGCGATCTC, *CACFD1*-csp2b: aaacGAG ATC GCG CAA GCT TGA AA, *CACFD1*-csp3a: CACGGGCTGTAGCTGCGCCTGA, *CACFD1*-csp3b: AAACCTCAGGCGCAGCTCACGGCC. Primers used for PCR to check deletion: *CACFD1*-PCR-csp1F: aagcttTAT GCT CCC TCT CCC ACA AGG C, *CACFD1*-PCR-csp1R: ctgcagGAC TGG ATA CTC ACA GAC TGC CC, *CACFD1*-PCR-csp2F: aagcttCTT CTG GGT GCT GTG AGA ACT GTG, *CACFD1*-csp2R: ctgcagGGA CGG CCA TGC ATT ACT CAC.

shRNAs. Stable knockdown of *hFWE* was performed using lentiviral constructs (Genscript) containing shRNA targeting *hFWE*. The shRNA sequences were: 5'-TCTGGCCTCTTCAACTGCATCACCATCCA-3'; 5'-TGAATGCC TTCATCTTGTGCTGTGTGAG-3'; 5'-CGTCTCTGGCAGAAAGGCTTCTCTACTAG-3'; and 5'-GGCAGCGGATGAGGAGAAGCTCGCG-3'. The lentiviral packaging was performed in 293FT cells using ViraSafe Lentivirus Packaging System (Pantropic Cell Biolabs), as per the manufacturer's instructions and previously stated. Forty-eight hours after transduction, cells were selected with 2 μ g ml⁻¹ puromycin in growth medium for 10 days and single colonies were selected and propagated. Gene knockdown efficiency was assessed by qPCR.

***hFWE* cDNA overexpression.** The pCDH-CMV-MCS-EF1 α -copGFP and pCDH-CMV-MCS-EF1 α -RFP vectors expressing individual *hFWE* isoforms 1–4 were obtained from System BioSciences. GFP-IRES-Isoform-1-4_OptHs vectors were obtained from ATUM. The lentiviral packaging was performed in 293FT cells using ViraSafe Lentivirus Packaging System (Pantropic Cell Biolabs) per the manufacturer's instructions.

MTT assay. We seeded 1 \times 10⁴ MCF-7 wild-type of *hFWE*^{KO} cells into 96-well plates overnight. Next, the culture medium was removed and cells were washed with PBS, and then incubated with 0.5 mg/ml 4,5-dimethylthiazol-2-yl-2,5-diphenyltetrazolium bromide (MTT; Sigma-Aldrich) in fresh culture medium for 3 h at 37 °C. The culture medium was carefully aspirated, and the formazan product was dissolved in 180 μ l DMSO. Cell viability was measured as the difference between the absorptions at wavelengths of 570 and 650 nm. All experiments were performed in triplicate and repeated three times.

Colony formation assay. MCF-7 wild-type and MCF-7 *hFWE*^{KO} cells were seeded into 6-well culture plates (1 \times 10³ cells per well) and then cultured under standard conditions over 21 days. The medium was replaced every third day. Finally, the cells were fixed with methanol and then stained with crystal violet (Sigma Aldrich). All experiments were performed in triplicate and replicated three times.

BrdU assay. Cellular proliferation was measured using the Cell Proliferation ELISA BrdU Colorimetric Assay Kit (Roche Applied Science). We plated 1 \times 10³ MCF-7 wild-type or *hFWE*^{KO} cells per well in 96-well plates. Twenty-four hours after plating, cells were labelled with BrdU in fresh culture medium overnight at 37 °C. Cells were then fixed and denatured for 30 min, followed by incubation with peroxidase substrate solution at 25 °C and the reaction was stopped using 1 M H₂SO₄. An absorbance wavelength of 450 nm and reference wavelength of 690 nm were used. All experiments were performed in triplicate and replicated three times.

ROS measurement. ROS levels were determined by incubating MCF-7 wild-type and *hFWE*^{KO} cells in serum-free DMEM containing 10 μ M 2',7'-dichlorodihydrofluorescein diacetate (H-DCFDA; Thermo Fisher Scientific) for 30 min at 37 °C. Cells were trypsinized and were washed twice in PBS, and the final cell pellet was re-suspended in PBS. DCF intensity was measured by flow cytometry using the BD-LSRII H274 per manufacturer's instructions. All experiments were performed in triplicate and replicated three times.

Apoptosis and cell cycle analysis. At the endpoint of monoculture or co-culture experiments, cells were stained with annexin-V (Thermo Fisher Scientific) per the manufacturer's instructions. Flow cytometry was performed to detect apoptotic cells by observing FITC-conjugated and Pacific blue-conjugated annexin-V staining. For cell cycle analysis, MCF-7 wild-type and MCF-7 *hFWE*^{KO} cells were fixed in 70% ethanol. Fixed cells were washed with cold PBS and stained with 50 μ g ml⁻¹ propidium iodide (Thermo Fisher Scientific). Flow cytometry for apoptosis detection and cell cycle distribution profiles was performed using MACSQuant Analyzer (Miltenyi Biotec) and analysed using FlowJo software (Treestar).

Live-cell imaging of cell competition assay. MCF-7 *hFWE*^{KO} cells were infected with lentiviral particles expressing GFP- or RFP-tagged *hFWE1*–*hFWE4* isoforms and cultured for 24 h. RFP⁺ and GFP⁺ cells were sorted by flow cytometry using the BD FACS ARIA III (BD Biosciences). Overexpression of *hFWE* in sorted cell populations was measured by qPCR and only sorted batches with high expression of *hFWE1*–*hFWE4* (characterized by *hFWE* Ct value of ~14, with *GAPDH* Ct value of ~21) were used. Equal numbers of MCF-7 cells expressing GFP- or RFP-tagged *hFWE1*–*hFWE4* were co-plated in a glass-bottom dish (Matek) in the specified combinations and co-cultured under normal conditions for 24 h. Cells were then subjected to live-cell imaging for the indicated times and processed for apoptosis detection by annexin-V staining. To study caspase-dependency for cell death, MCF-7 *hFWE*^{KO} cells expressing *hFWE*^{win} were co-cultured with MCF-7 *hFWE*^{KO} cells expressing *hFWE*^{lose} in the presence of the caspase inhibitor Z-VAD-FMK (20 μ M, Sigma-Aldrich) for 24 h. We next performed live-cell imaging at the indicated times, and, at the study endpoint, cells were processed for apoptosis detection by annexin-V staining when indicated. To observe the contact-dependency of cell competition, an equal number of MCF-7 *hFWE*^{KO} cells expressing *hFWE1*–GFP and MCF-7 *hFWE*^{KO} cells expressing *hFWE2*–RFP were co-plated at low density, followed by live-cell imaging. For conditioned medium experiments, medium was collected from MCF-7 *hFWE*^{KO} cells expressing *hFWE2* cDNA, centrifuged at 1,000 r.p.m. for 5 min, and then added to target MCF-7 *hFWE*^{KO} cells expressing *hFWE1*–GFP. Cells were subsequently cultured for 24 h, then we performed live-cell imaging at the indicated times. Live-cell imaging was performed using Leica TCS SP8 confocal laser microscopy (Leica Microsystems), a Nikon A1 HD25 confocal microscope (Nikon), and a Zeiss LSM-800 with Airy Scan Confocal Microscope (Zeiss). Analysis of cell motility, cell count and cell death was performed manually using Fiji software (<http://fiji.sc/>) and the analysis of average cell volume and average cell sphericity were performed using Imaris7.6.5 software (Bitplane).

Cell competition assay with normal breast cells. MCF-7 *hFWE*^{KO} cells were infected with lentiviral particles expressing *hFWE2*–GFP and cultured for 24 h. MCF-7 *hFWE*^{KO} cells expressing *hFWE2*–GFP were subsequently cultured on their own or co-cultured with an equal number of normal breast primary epithelial cells or fibroblasts. Cells from each combination were collected at the indicated times for annexin-V staining and the percent of apoptotic cells was measured in the GFP-positive and GFP-negative populations using flow cytometry. Human epithelial cells and fibroblasts were isolated from normal breast tissue from fresh or cryopreserved, de-identified tissues; samples were obtained from the Komen Tissue Bank (KTB) at IU School of Medicine, Indianapolis, after informed consent from the donors. All experiments were carried out in accordance with the approved guidelines of the Indiana University Institutional Review Board, which determined the study to be non-human subjects research. International Ethical Guidelines for Biomedical Research Involving Human Subjects were followed. Procedures for isolation of primary cells from biopsies and propagation have been described³³.

Determination of cellular calcium levels. MCF-7 *hFWE*^{KO} cells and MCF-7 *hFWE*^{KO} cells infected with lentiviral particles expressing *hFWE1*–4 isoforms

individually were plated in glass-bottom dishes (Matek). After 24 h, cells were incubated with the fluorescent dye Fluo-4AM (Thermo Fisher Scientific) as per the manufacturer's protocol for 40 min, washed with PBS, and then incubated for an additional 15 min to complete the de-esterification of the dye. Live-cell imaging was immediately performed at the indicated times to determine cellular Ca^{2+} levels using TCS SP8 (Leica) confocal imaging. An excitation wavelength of 494 nm and an emission wavelength of 506 nm were used. Results were quantified by measuring the Ca^{2+} indicator mean fluorescence intensity (MFI) in all cell combinations using Fiji. All experiments were performed in triplicate and repeated three times. **BAPTA-AM.** MCF-7 *hFWE^{KO}* cells were infected with lentiviral particles expressing hFWE1-RFP or hFWE2-GFP and cultured for 24 h. Then, MCF-7 *hFWE^{KO}* cells expressing hFWE1-RFP and MCF-7 *hFWE^{KO}* cells expressing hFWE2-GFP were co-plated in equal numbers and co-cultured for 24 h in the presence or absence of BAPTA-AM (10 μ M, Thermo Fisher Scientific). Cells were collected for annexin-V staining and flow cytometry analysis.

Laser-capture microdissection. FFPE tissue sections (5- μ m thick) were subjected to laser capture microdissection using the Leica Microsystems at UNMC; Zeiss Palm MicroBeam IV Laser Capture Microdissection system at Thornwood facility and Michigan University. Matched H&E-stained sections were used to demarcate cancer versus stroma. Adjacent normal tissues were microdissected in precise increments of 200 μ m in distance perpendicular from the boundary of tumour mass. Captured tissue was collected into the adhesive cap (Zeiss).

Immunohistochemistry. Matched normal and tumour patient samples of breast and colon origin were formalin-fixed and paraffin-embedded. FFPE tissues were cut into sections of 5 μ m and were stained with H&E or hFWE antibodies. Samples were deparaffinized in xylene and rehydrated in a graded series of ethanol. Antigen retrieval was performed in 10 mM EDTA buffer pH 9 for 20 min at 96–98 °C. Samples were allowed to cool at room temperature for 20 min, and blocked in 1% peroxide solution for 10 min, followed by washing with TBS + 0.5% Triton X-100. Slides were blocked in 3% bovine serum albumin (BSA, Sigma-Aldrich), then incubated with anti-hFWE-N-term (Ab1; 1:500) and anti-hFWE^{Win} (Ab4; 1:500) primary antibodies (Genscript) in blocking solution overnight at 4 °C. The sections were incubated in goat anti-mouse IgG HRP-conjugated secondary antibody (1:2,000, Thermo Fisher Scientific) for 1 h at 25 °C and then developed with 3,3'-diaminobenzidine (DAB, Vector Labs) for 10 min to visualize the colour of the reaction.

Immunofluorescence. For immunofluorescent and immunocytological staining for hFWE in human tissue and cells, anti-hFWE-N-term (Ab1) and anti-hFWE^{Win} (Ab4) antibodies were used at 1:500 final dilution, and goat anti-mouse IgG AlexaFluor 488 (1:1,000, Thermo Fisher Scientific) was used as the secondary antibody. SCC, colon, and normal skin FFPE samples were cut into 5- μ m sections and stained with H&E or hFWE antibodies. Immunofluorescence experiments were performed as described previously³⁴ and refined for the hFWE antibodies. Serial sections were incubated with anti-hFWE-N-term and anti-hFWE^{Win} antibodies overnight at 4 °C. Sections were incubated with secondary antibody for 2 h and nuclei were counterstained with 4',6-diamidino-2-phenylindole (DAPI, Sigma-Aldrich, 1 μ g ml⁻¹).

Immunocytochemistry. MCF-7 *hFWE^{KO}* cells and MCF-7 *hFWE^{KO}* cells expressing one of hFWE1–hFWE4 were collected by trypsinization and the cell pellet was resuspended in pre-heated 1.5% agarose + 2% sucrose solution, homogenized, and allowed to solidify. The agarose block was placed in 30% sucrose overnight. Eight-micrometre-thick sections were prepared using a Cryostat 3050S (Leica) and slides were stained using the Bond Polymer Refine Detection Kit (Leica) per the manufacturer's instructions. Slides were then incubated with anti-hFWE-N-term and anti-hFWE^{Win} antibodies for 15 min and subsequently processed using Leica Detection Polymer and developed with DAB according to the kit instructions.

To analyse the membrane topology of hFWE isoforms, MCF-7 *hFWE^{KO}* cells were plated in Nunc LabTek-II 4-chambered coverglass (Thermo Fisher Scientific) overnight and then transfected with cDNA for hFWE1–hFWE4 using Lipofectamine 3000. After 24 h, the cells were fixed with 3.7% paraformaldehyde in PBS for 15 min, and then permeabilized with 0.1% Triton X-100 in TBS for 7 min or non-permeabilized. Subsequently, the cells were blocked with 3% BSA and incubated with anti-hFWE-N-term or anti-hFWE^{Win} primary antibody in 3% BSA for 4 h, washed three times with 1 \times PBS and stained with secondary antibody for 2 h. Nuclei were counterstained with Hoechst 33258 (Thermo Fisher Scientific). Images were acquired with a Zeiss LSM880 inverted by using a Plan-ApoChromat 20 \times /0.8 dry lens. An argon laser with 25 mW of head power and a 405 Diode laser with 30 mW head power were used to excite AlexaFluor488 and Hoechst, respectively. The signal detected was limited to the portions of the visible spectrum between 495 and 545 nm and 420 and 480 nm by using BP filters in front of a ZEISS Airy Scan detector. The images were acquired in super-resolution mode with an XY sampling factor (pixel size) of 55 nm. A volume of approximately 12 μ m was acquired around the central plane of each cell with a z-step of 342 nm. After the acquisition, the images were processed in order to reassign the information

collected by the 32 Airy detectors to their source point and obtain a theoretical resolution of 233 nm for the A488 channel and 204 nm for the Hoechst channel.

Fluorescent in situ hybridization. FFPE breast cancer sections (5- μ m thick) were stained with H&E to verify that the slides included both cancer and normal tissue. Next, 5- μ m-thick serial sections were prepared for processing with the in situ + ISH Tissue Assay kit (Affymetrix) according to the manufacturer's instructions. Probe sets were designed by Affymetrix to detect exon 3 and exon 4 of *CACFD1* mRNA. After deparaffinization, slides were subjected to heat pretreatment (90 °C, 30 min) and protease digestion, (40 °C, 20 min). Then sections were hybridized with probe following the signal-amplification step. Sections were developed using kit-supplied Fast Red substrate and counterstained with DAPI. All sections were mounted with DAKO UltraMount Permanent Mounting Medium (Agilent). Fluorescent images were acquired using a BZ-X700 microscope (Keyence).

RNA isolation and quantitative RT-PCR analysis. Total RNA was isolated from cancer cell lines, patient tumour samples, and mouse tumour xenografts using the PureLink RNA Mini kit (Qiagen). Total RNA was isolated from laser-captured FFPE tissue samples using the RNeasy FFPE kit (Qiagen). Ten nanograms of total RNA was reverse-transcribed to complementary DNA using Superscript Vilo cDNA synthesis kit (Thermo Fisher) per the manufacturer's instructions. Quantitative PCR (qPCR) was performed with PowerUp SYBR Green master mix (Thermo Fisher) using the Rotor Gene Q (Qiagen), BioRad CFX96, QuantStudio 6 (ABI) or Light cycler 96 instrument (Roche). The reaction conditions included an initial denaturation step at 95 °C for 2 min, followed by 40 cycles of 95 °C for 15 s and 60 °C for 60 s. Data were analysed using the comparative C_t method³⁵. The C_t values of samples and controls were normalized to the expression level of the *GAPDH* housekeeping gene. All qPCR reactions were set up in triplicate and the experiments were performed with at least three different samples. The following primers were used (F: forward; R: reverse): *GAPDH*: 5'-GGATGCAGGATGATGTTT-3' (F) and 5'-TGCACCACCAACTGCTTAG-3' (R); *hFWE1*: Ex2–4 5'-GCGTGTGGATGATGATGG' (F) and Ex5 5'-CCTGTCTTGTCCCCTTGA-3' (R); *hFWE2*: Ex3 5'-CTGCCAGTTCATCGAGTTT-3' (F) and Ex5 5'-CCTGTCTTGTCCCCTTGA-3' (R); *hFWE3*: Ex2–4 5'-GCGTGTGGATGATGATGG-3' (F) and Ex4–6 5'-AGATCGCATCGCCCTTT-3' (R); *hFWE4*: Ex3 5'-CTGCCAGTTCATCGAGTTT-3' (F) and Ex4–6 5'-GATCGCATCGCCCTTTT-3' (R); *hFWE^{Win}*: 5'-GCCTTCATCTTGTGTGTG-3' (F) and 5'-CATCCCAGTAGAAGACAG-3' (R); *hFWE^{Loss}*: 5'-GCGTGTGGATGATGATGG-3' (F) and 5'-AGCAGAGAGTCCGTACA GCA-3' (R); mouse *Fwe1* 5'-TCCACTTCTCTGTTCTG-3' (F) and 5'-GTGAGTACTGC TGTC TAGCC-3' (R); mouse *Fwe2* 5'-CGATGCCATTTCTTATGCTC-3' (F) and 5'-TGACATCAGTCTTCTCCAG-3' (R); mouse *Fwe3* 5'-CAAA CACAGATCTGAGAAGG-3' (F) and 5'-TAGAGGAAATGGTGTCT G-3' (R); mouse *Fwe4* 5'-GTTTGCTAAATCCTGGGTGTC-3' (F) and 5'-GCGTTCATGATCATCCACAC-3' (R); mouse *Gapdh* 5'-GTATGT CGTGGAGTCTACTG-3' (F) and 5'-TCATCATACTTGGCAGGTTT-3' (R) as described previously²⁶.

The human apoptosis PCR array. The Human Apoptosis RT2 Profiler PCR array kit (PAHS-3012; SA-Bio Sciences) was used to profile the expression of 354 genes involved in apoptosis and qPCR was performed per the manufacturer's instructions.

Epithelial cell isolation. hFWE^{Win} expression was observed in the total normal tissue and the epithelial fraction isolated from breast, colon, and lung tissue samples. All samples were purchased from Tissue For Research, UK (<https://biobankonline.com/>) and all tissue samples were procured with donor consent. For extraction of the epithelial cells, approximately 120–150 g of the normal tissue samples were used as starting material for tissue digestion. Samples were handled in sterile conditions. Fatty tissue was manually separated, using sterile scalpels and forceps. Subsequently, the epithelial-enriched tissue was manually minced into small pieces. The tissue was sequentially digested using a slow digestion process (overnight at low enzymatic concentration) followed by sequential filtering to support the growth of the epithelial cell fractions as described previously³⁶.

Patient samples. For FISH, breast tumour specimens were provided by the Department of Breast Surgery, Hokkaido University Hospital. For qPCR experiments, samples of benign (10 breast and 10 colon) and malignant tumour (25 breast and 21 colon) were provided by the Department of Pathology, UAMS, USA; samples of malignant lung (4) and normal tissue (2 lung and 1 skin) were procured from the Department of Pathology, Locarno Hospital, Switzerland; and samples of SCC (3) and normal skin (2) were obtained from the Department of Pathology, Creighton University School of Medicine, USA. The same set of normal and malignant SCC samples were also used for immunofluorescent staining. FFPE breast and colon cancer samples used for immunohistochemistry (IHC) and fresh normal breast samples were provided by the Pathology Department, Champalimaud Foundation.

All samples used in the study were de-identified, FFPE archived samples with no attached patient information, and were collected with informed consent from donors. All samples were reviewed by the IRB boards at UAMS, Hokkaido

University Hospital, Locarno Hospital, Creighton University School of Medicine, Champalimaud Foundation and determined to qualify as non-human subjects research.

Cancer xenografts. C57BL/6 mice were obtained from the Geisel School of Medicine, Dartmouth College. Male and female Swiss nude mice were purchased from Charles River. All animal protocols were approved by the Institutional Animal Care and Use Committee of Dartmouth, and the Institutional Animal Ethics Committee at Champalimaud Foundation. All mice were housed in laminar flow cabinets under specific pathogen-free conditions. Food and water were available ad libitum for the duration of the studies. *Fwe*^{KO} mice were generated using female C57BL/6 mice as described earlier¹. For the generation of tumours in C57BL/6 mice, cyclosporin A (30 mg kg⁻¹; Sigma-Aldrich) was injected intraperitoneally as described³⁷. Cell line xenografts were established as described previously^{38–40}. In brief, MCF-7, HCT-116, DU-145, CCL-218, and OVCAR-8 cells at 70–90% confluency were trypsinized and cell viability, required to be at least >95%, was determined by Trypan blue exclusion assay. Cells were re-suspended in 80 μ l serum-free medium with 1:1 Matrigel at a final concentration of 1×10^6 cells ml⁻¹ and stored on ice. For all tumour cell injections, animals were first anaesthetized with 1.5–3% isoflurane with 30% oxygen.

For overexpression of individual hFWE isoforms in mouse mammary tissue, 50 μ l lentiviral particles (10^{11} TU ml⁻¹) expressing individual GFP-tagged hFWE1–hFWE4 isoforms were injected into the mammary tissue of immunosuppressed C57BL/6 *Fwe*^{KO} mice as described⁴¹. For injection of MCF-7 *hFWE*^{KO} cells expressing GFP-tagged hFWE1–hFWE4, a pellet of 17- β -oestradiol (0.18 mg per pellet, 60-day release; Innovative Research of America) was subcutaneously implanted into *Fwe*^{KO} mice 3 days before cell injection. One week after lentiviral treatment, MCF-7 *hFWE*^{KO} cells expressing GFP-tagged hFWE1–hFWE4 were injected into the mammary tissue. After 4 weeks, mice were monitored for bioluminescent signal using an IVIS 200 system (Xenogen).

For cell line xenograft tumour studies established in male and female Swiss athymic nude mice (age 4–6 weeks), an 80- μ l cell suspension containing 1×10^6 cells was subcutaneously injected into the hind legs of athymic mice. The vehicle control used for these studies was DMSO. To rescue hFWE2 expression in HCT-116 *hFWE*^{WT} tumours, 14 days after cell line injection, tumour-bearing mice were randomly selected and lentiviral particles expressing hFWE2 were injected directly into the established tumour as described previously^{42,43}. Chemotherapy treatments were initiated when tumours reached an approximate size of 0.03 cm³; tumour-bearing mice were randomized to receive 30 mg kg⁻¹ 5-FU as described²⁸ or 4 mg kg⁻¹ cisplatin + docetaxel as described³⁰. Tumour volumes were carefully monitored after treatment using Vernier caliper measurements of length, width, and height, and volumes were calculated using the formula for a semi-ellipsoid ($4/3\pi r^3/2$), as described previously^{38,44}. Tumour size did not exceed the maximum size of 1.28 cm³ as specified by institutional policies. The investigators were blinded during experiments or outcome assessment. No statistical methods were used to predetermine sample size.

Statistical analysis. All values are expressed as means \pm s.d. of independent experiments. Differences between groups were evaluated by Student's *t*-test (two-sided) or Tukey–Kramer test, and considered to be significant at $P < 0.05$.

Reporting summary. Further information on research design is available in the Nature Research Reporting Summary linked to this paper.

Data availability

All data generated or analysed during this study are included in the paper, its Extended Data and its Supplementary Information. The source data for Figs. 2–4 and Extended Data Figs. 1–10 are available online.

- Sanjana, N. E., Shalem, O. & Zhang, F. Improved vectors and genome-wide libraries for CRISPR screening. *Nat. Methods* **11**, 783–784 (2014).
- Shalem, O. et al. Genome-scale CRISPR-Cas9 knockout screening in human cells. *Science* **343**, 84–87 (2014).
- Prasad, M. et al. Dual TGF β /BMP pathway inhibition enables expansion and characterization of multiple epithelial cell types of the normal and cancerous breast. *Mol. Cancer Res.* **17**, 1556–1570 (2019).
- Yanagida, J. et al. Accelerated elimination of ultraviolet-induced DNA damage through apoptosis in CDC25A-deficient skin. *Carcinogenesis* **33**, 1754–1761 (2012).

- Schmittgen, T. D. & Livak, K. J. Analyzing real-time PCR data by the comparative C(T) method. *Nat. Protoc.* **3**, 1101–1108 (2008).
- Zubeldia-Plaazaola, A. et al. Comparison of methods for the isolation of human breast epithelial and myoepithelial cells. *Front. Cell Dev. Biol.* **3**, 32 (2015).
- Jivrajani, M., Shaikh, M. V., Shrivastava, N. & Nivsarkar, M. An improved and versatile immunosuppression protocol for the development of tumor xenograft in mice. *Anticancer Res.* **34**, 7177–7183 (2014).
- Gogna, R., Madan, E., Kuppasamy, P. & Pati, U. Chaperoning of mutant p53 protein by wild-type p53 protein causes hypoxic tumor regression. *J. Biol. Chem.* **287**, 2907–2914 (2012).
- Hadjal, Y., Hadadeh, O., Yazidi, C. E., Barruet, E. & Binétruy, B. A p38MAPK-p53 cascade regulates mesodermal differentiation and neurogenesis of embryonic stem cells. *Cell Death Dis.* **4**, e737 (2013).
- Madan, E. et al. SCO2 induces p53-mediated apoptosis by Thr845 phosphorylation of ASK-1 and dissociation of the ASK-1-Trx complex. *Mol. Cell. Biol.* **33**, 1285–1302 (2013).
- Annunziato, S. et al. Modeling invasive lobular breast carcinoma by CRISPR/Cas9-mediated somatic genome editing of the mammary gland. *Genes Dev.* **30**, 1470–1480 (2016).
- Akhtar, J., Wang, Z., Yu, C. & Zhang, Z. P. Effectiveness of local injection of lentivirus-delivered stathmin1 and stathmin1 shRNA in human gastric cancer xenograft mouse. *J. Gastroenterol. Hepatol.* **29**, 1685–1691 (2014).
- Zheng, J. Y. et al. Regression of prostate cancer xenografts by a lentiviral vector specifically expressing diphtheria toxin A. *Cancer Gene Ther.* **10**, 764–770 (2003).
- Madan, E. et al. TIGAR induces p53-mediated cell-cycle arrest by regulation of RB-E2F1 complex. *Br. J. Cancer* **107**, 516–526 (2012).

Acknowledgements This study was supported by ERC, SNSF, Josef Steiner Cancer Research Foundation, Swiss Cancer League and Champalimaud Foundation to E.M.; and Swiss Cancer League, LB692, LB506, Seeds of Science, Winthrop P Rockefeller Cancer Institute and Creighton University startup funds to R.G. We thank K. Polyak for experimental suggestions; J. Billheimer and A. Dhiman for help with analysis; A. Gogna for support; and the MTT platform (R. Tomás), the Histopathology Platform (I. Terras Marques, M. I. Romano, S. Casimiro and S. Dias) and the Rodent platform at the Champalimaud Centre for the Unknown.

Author contributions R.G. and E. Moreno conceptualized the idea, initiated the project, provided research support, designed, analysed, and interpreted the experiments and wrote the manuscript. E. Madan analysed the experiments, wrote the manuscript, and performed imaging, qPCR, flow-cytometry and mouse studies. R.G. designed and analysed the experiments, wrote the manuscript, created molecular biology design, and performed imaging analysis, clonogenicity assay, FISH-molecular design, IHC, mouse studies, and chemotherapy designs. C.J.P. analysed the experiments, helped in the preparation of figures, formatted and wrote the manuscript and performed statistical analysis, cell culture experiments, calcium imaging, low-density plating and conditioned medium experiments, and knockout and wild-type cell interactions. M.N. analysed the experiments, helped in the preparation of figures, and performed statistical analysis, flow-cytometry experiments and analysis, and FISH. T.M.P. analysed the experiments, helped in preparation of figures, formatted and wrote the manuscript, performed statistical analysis and cell culture experiments, extracted and cultured normal and epithelial cells from breast tissue, and performed laser-capture microdissection, qPCR, flow-cytometry and virus production. R.C.-M., A.G., V.H., Y.Y., T.Y., D.S., S.R.P. and H.Y. assisted in procuring tissue samples and IHC. K.F. performed IHC. K.S., A.M.P. and D.C. assisted with experiments and analysis. C.R. assisted with manuscript writing. M.A.F.P. and A.V. assisted with flow-cytometry experiments. D.A. assisted with confocal microscopy. H.N. provided normal breast cells. L.A.H. provided SCC samples, supervised K.F. for IHC in SCC and edited the manuscript. P.K. provided research support, and helped with data analysis, organization, and editing of the manuscript. C.C. and A.L.B. provided a clinical perspective, and helped with the procurement of tissue samples, design of IHC experiments, and design of clinical experiments such as the inclusion of chemotherapy.

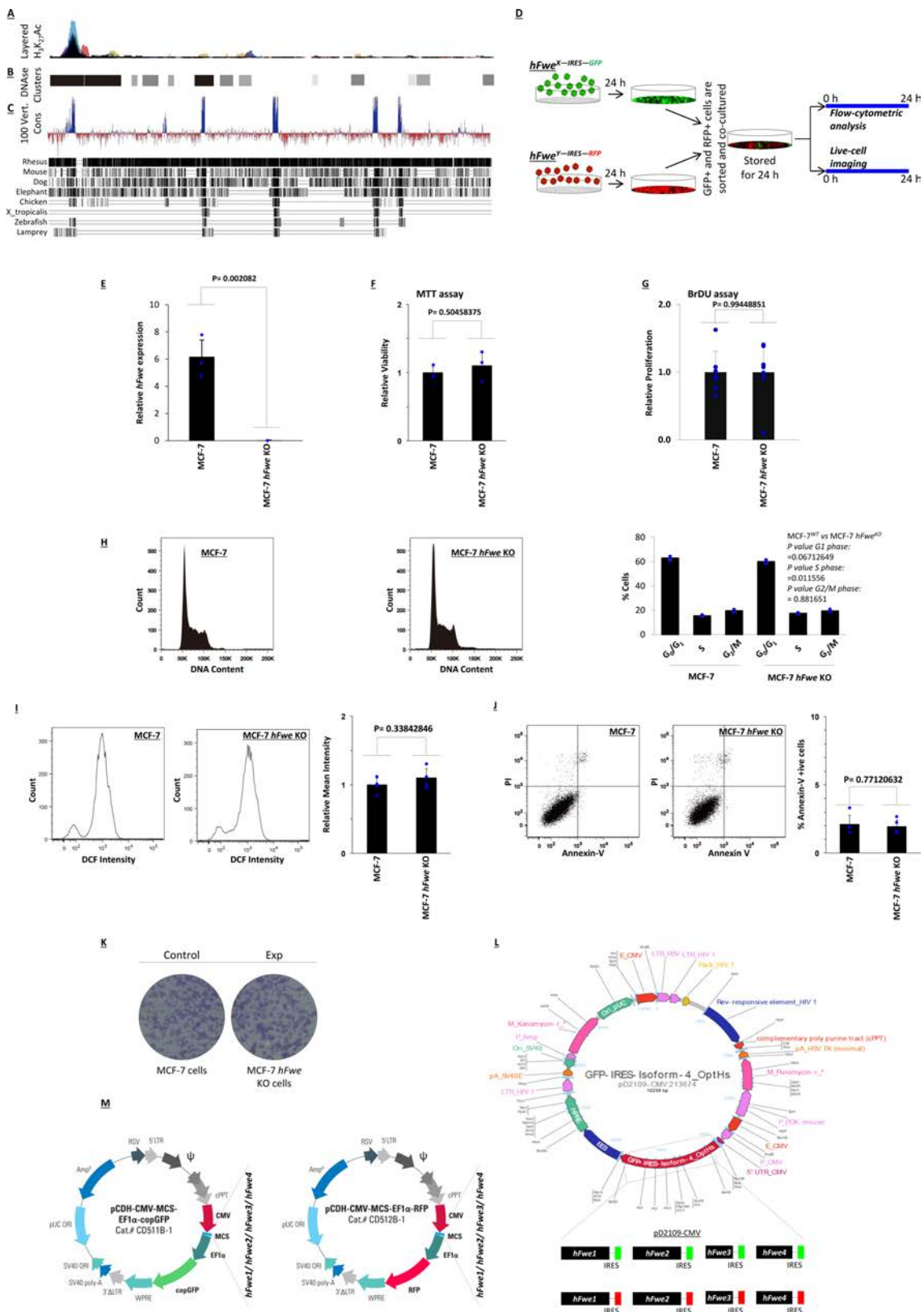
Competing interests : The authors declare no competing interests.

Additional information

Supplementary information is available for this paper at <https://doi.org/10.1038/s41586-019-1429-3>.

Correspondence and requests for materials should be addressed to R.G. or E. Moreno

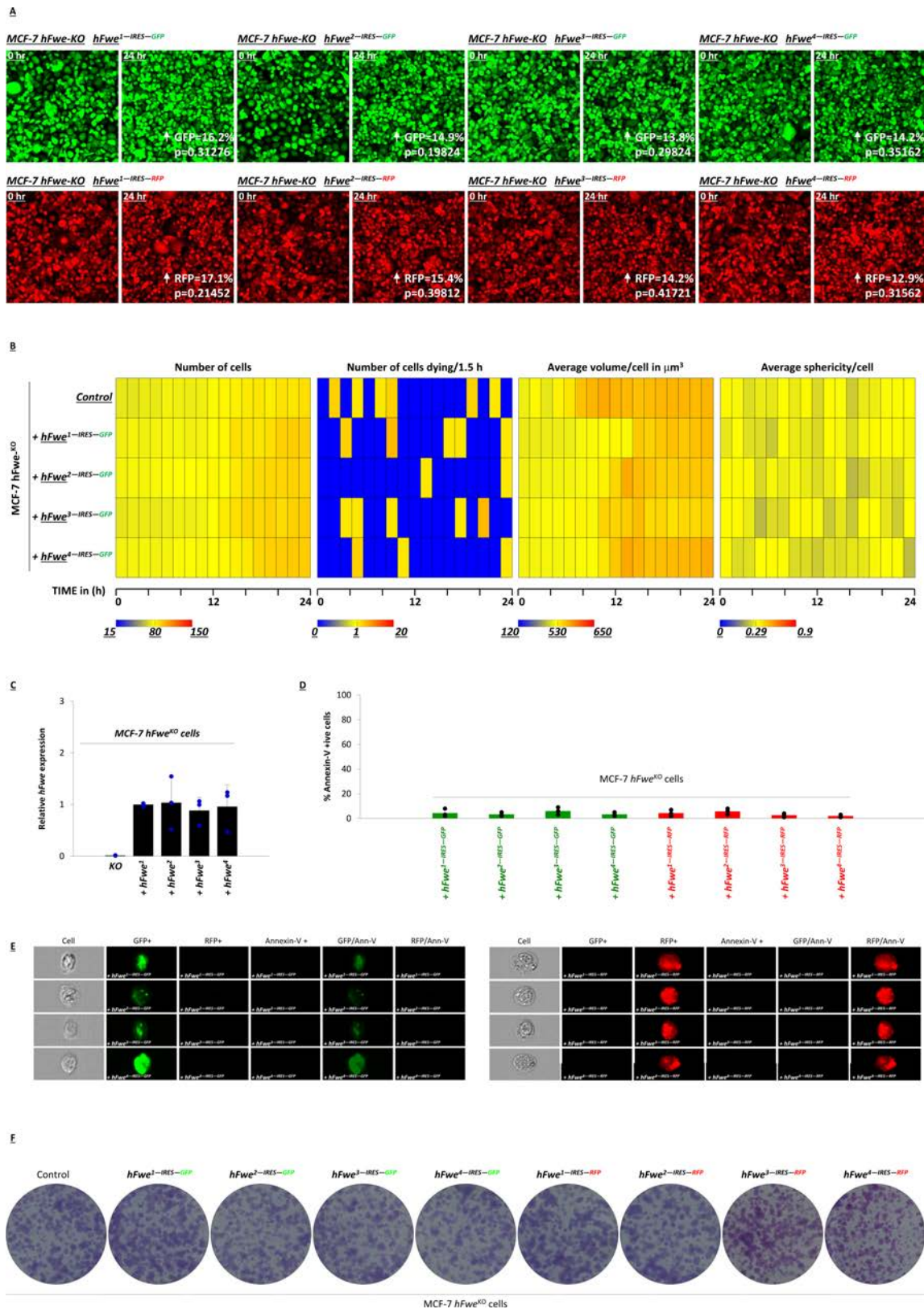
Reprints and permissions information is available at <http://www.nature.com/reprints>.



Extended Data Fig. 1 | See next page for caption.

Extended Data Fig. 1 | Knockout of the *hFWE* gene in MCF-7 cells does not affect their cellular functions. **a**, ENCODE data mining for chromatin immunoprecipitation (ChIP) with H₃K₂Ac antibody shows active euchromatin status of the *hFWE* promoter. **b**, ENCODE data mining for DNAase-I hypersensitivity analysis shows footprints of DNA unwinding at the locations of *hFWE* exons. **c**, Phylogenetic analysis. Exon sequences are highly conserved amongst vertebrates except exon 5, which is more specific to mammals. **d**, Pictorial representation of the protocol for the functional analysis of *hFWE* isoforms in cell culture. MCF-7 *hFWE*^{KO} cells were infected with lentiviruses encoding each *hFWE* isoform alongside an independent GFP or RFP tag. Transduced cells were sorted for RFP⁺ and GFP⁺ populations, plated together and co-cultured for 24 h. Co-cultured cells were then studied for a further 24 h using live-cell imaging and flow cytometry. **e**, To obtain human cells expressing single *hFWE* isoforms, MCF-7 cells (breast cancer origin) were selected and MCF-7 *hFWE*^{KO} cells were generated. qPCR analysis of relative transcript synthesis of *hFWE* exon 1 from MCF-7 *hFWE*^{WT} and MCF-7 *hFWE*^{KO} cells shows lack of gene product in the knockout cells ($n = 3$ biologically independent experiments). **f**, MTT assay shows that knockout of the *hFWE* gene does not affect cell viability and mitochondrial activity in MCF-7 cells ($n = 3$ biologically independent experiments). **g**, BrdU

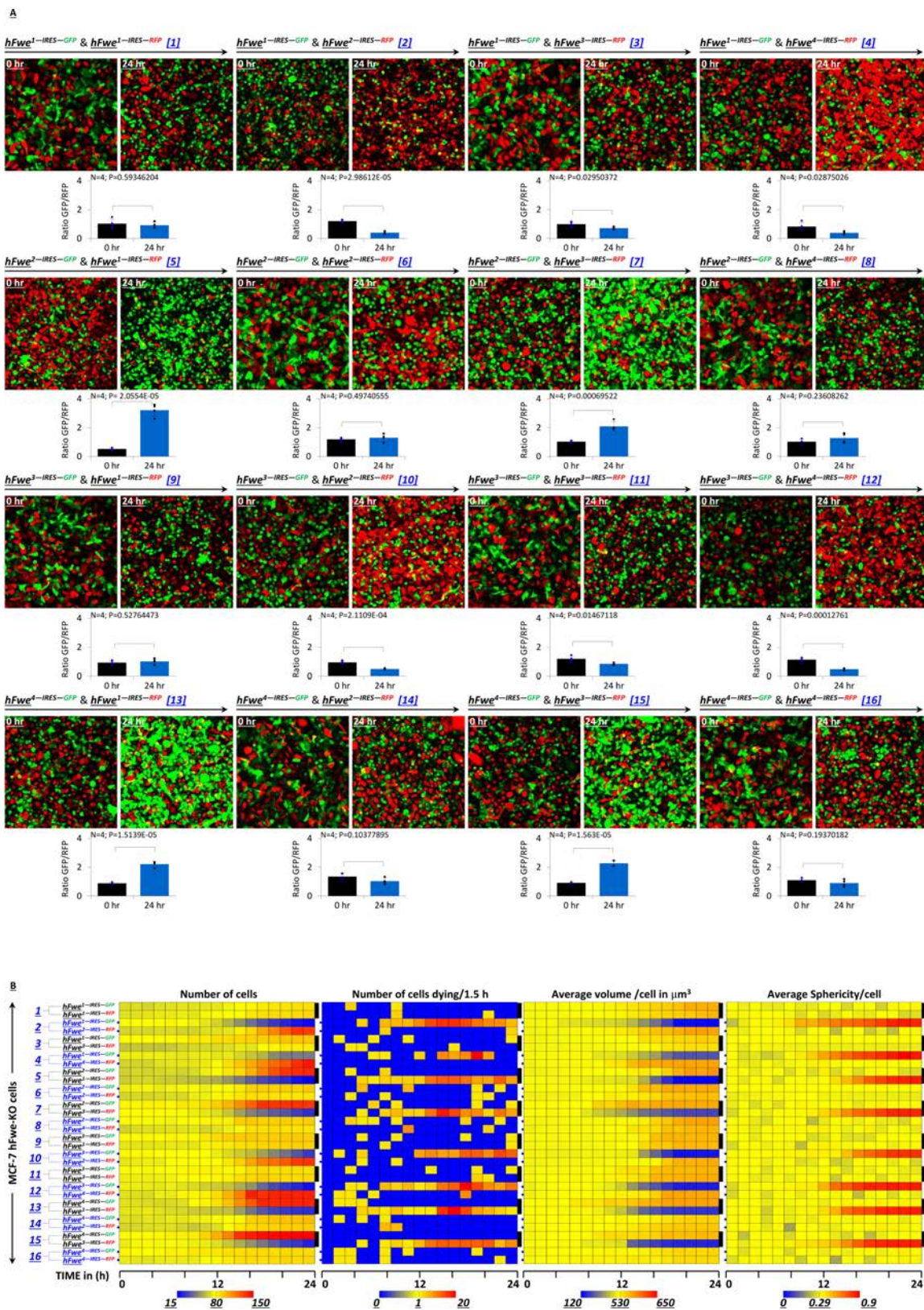
assay shows that knockout of the *hFWE* gene does not affect cellular proliferation rates of MCF-7 cells ($n = 7$ biologically independent experiments). **h**, Cell-cycle distribution was examined by analysing DNA content. Propidium iodide staining and subsequent flow cytometric analysis show that knockout of the *hFWE* gene does not affect the cell-cycle progression of the MCF-7 cells ($n = 3$ biologically independent experiments). **i**, Flow cytometric analysis of ROS via measurement of DCF fluorescence shows that knockout of the *hFWE* gene does not alter cellular ROS in MCF-7 cells ($n = 4$ biologically independent experiments). **j**, Annexin-V staining shows that knockout of the *hFWE* gene does not affect cellular apoptosis in MCF-7 cells ($n = 4$ biologically independent experiments). **k**, The clonogenic assay shows that knockout of the *hFWE* gene does not affect the ability of MCF-7 cells to form colonies ($n = 3$). **l**, Diagrammatic representation of the *hFWEX*-IRES-GFP/RFP lentiviral constructs. Eight lentiviral constructs were prepared by cloning *hFWE1/2/3/4*-IRES-GFP/RFP into pD2109-CMV lentiviral vectors. **m**, Eight additional constructs were prepared by cloning *hFWE1/2/3/4* into dual promoter pCDH-CMV-MCS-EF1 α -copGFP and pCDH-CMV-MCS-EF1 α -copRFP (System Biosciences), respectively. **e-j**, P values shown, two-tailed t -test, mean \pm s.d.



Extended Data Fig. 2 | See next page for caption.

Extended Data Fig. 2 | Overexpression of single hFWE isoforms in MCF-7 *hFWE*^{KO} cells does not alter viability. **a**, MCF-7 *hFWE*^{KO} cells were infected with each *hFWE1/2/3/4-GFP/RFP* construct independently and the cells were monitored via live-cell imaging. Images at 24 h show that MCF-7 *hFWE*^{KO} cells homogenously expressing single hFWE isoforms do not undergo cell death ($n = 3$ biologically independent experiments, P values shown, two-tailed t -test). **b**, Analysis of live-cell imaging is shown as heat maps to represent the total number of cells, number of cells dying every 1.5 h, average cellular volume and average cellular sphericity; each block represents a gradient scale of low (blue), medium (yellow) and high (red) number or shape or size of the cells ($n = 3$, analysis performed using manual tool from Fiji and automated tools from Imaris, Genie tool used for representing data as heat maps). **c**, qPCR analysis of MCF-7 *hFWE*^{KO} cells expressing each of four hFWE isoforms showed comparable

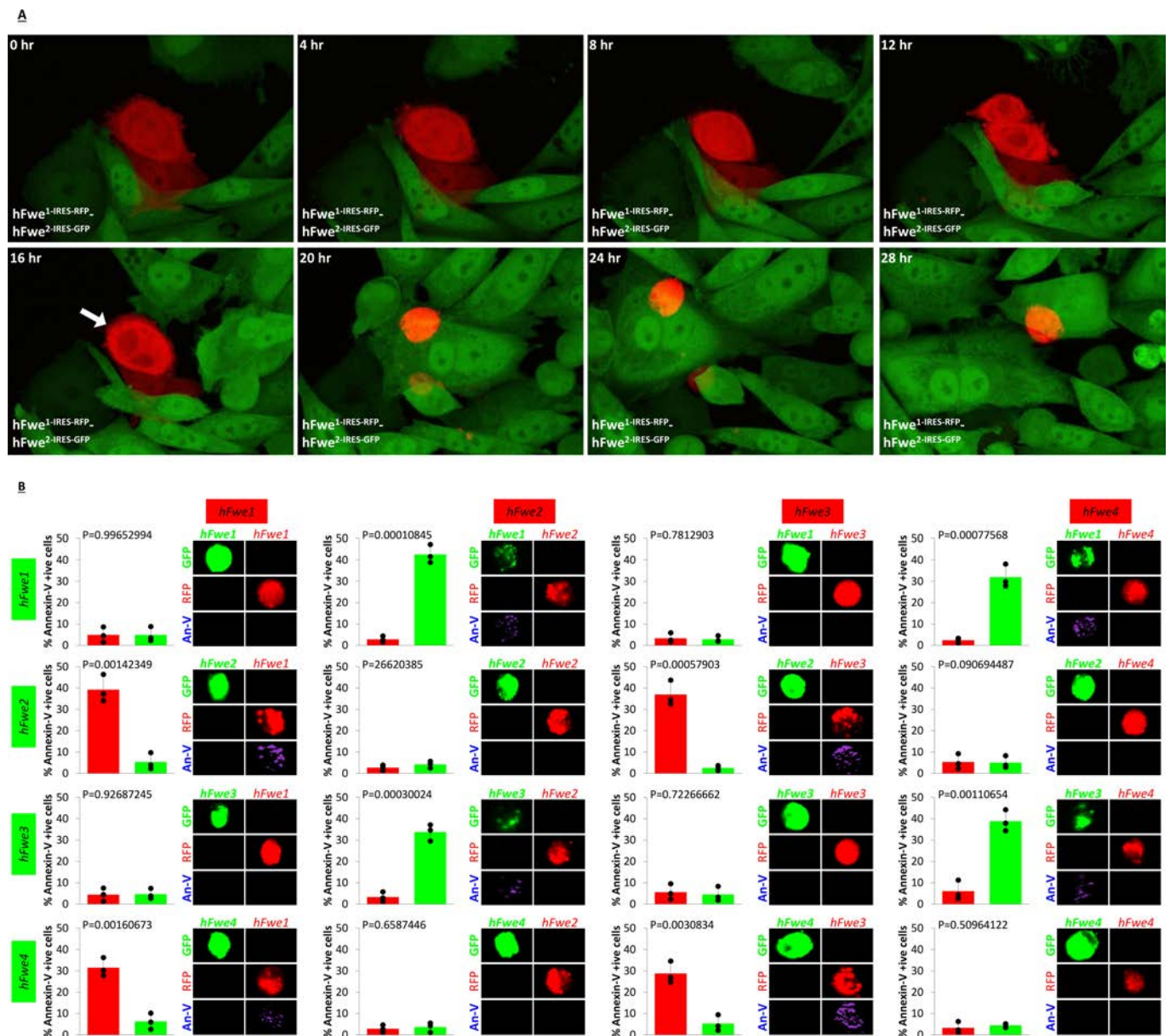
lentiviral-mediated expression of hFWE1, hFWE2, hFWE3 or hFWE4 ($n = 3$ biologically independent experiments, mean \pm s.d., ANOVA showed no significant differences). **d**, Flow cytometry-based annexin-V staining shows that overexpression of individual hFWE1/2/3/4-GFP/RFP isoforms does not induce apoptosis in MCF-7 *hFWE*^{KO} cells ($n = 3$ biologically independent experiments, mean \pm s.d., ANOVA showed no significant differences). **e**, Annexin-V staining and flow cytometry-based cell imaging (image stream) also show that overexpression of individual hFWE isoforms does not induce apoptosis ($n = 3$). **f**, Long-term effect of overexpression of single hFWE isoforms with GFP or RFP reporters over 21 days using clonogenic assay. The overexpression of hFWE isoforms does not affect the colony formation ability of MCF-7 *hFWE*^{KO} cells ($n = 3$).



Extended Data Fig. 3 | See next page for caption.

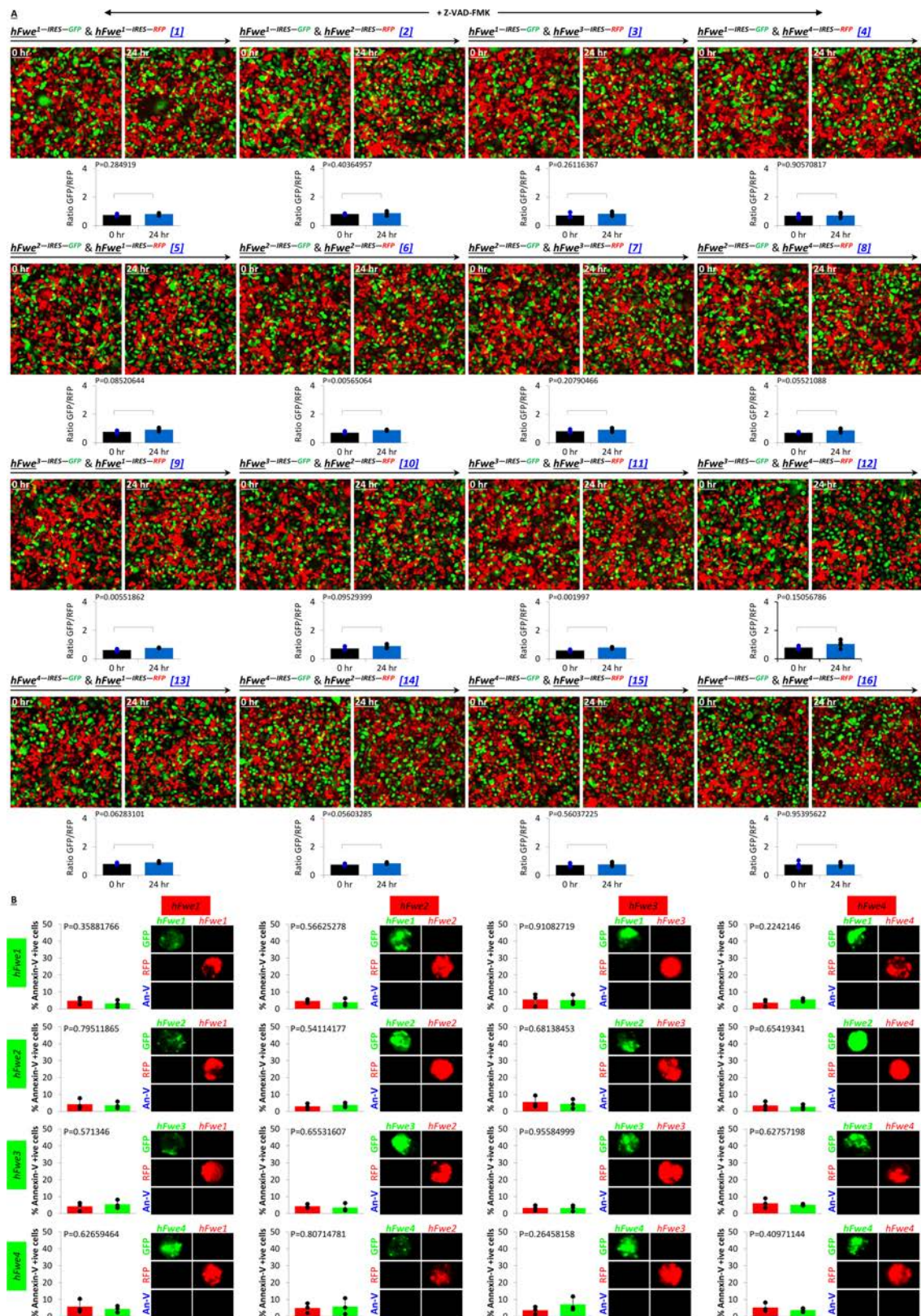
Extended Data Fig. 3 | Live-cell imaging of co-culture assay using MCF-7 *hFWE*^{KO} cells transduced with hFWE isoforms. **a**, Results from 24-h live-cell imaging experiments of co-cultures of MCF-7 *hFWE*^{KO} cells expressing the four hFWE isoforms. In [1], MCF-7 *hFWE*^{KO} cells expressing hFWE1–IRES–GFP were co-cultured with cells expressing hFWE1–IRES–RFP. GFP⁺ and RFP⁺ cells were monitored at 0 and 24 h to follow the effects of hFWE isoforms on cell proliferation. The ratio of GFP⁺ to RFP⁺ cells did not vary significantly between 0 and 24 h. In co-culture experiments [2], MCF-7 *hFWE*^{KO} cells expressing hFWE1–IRES–GFP were co-cultured with cells expressing hFWE2–IRES–RFP. The population of RFP⁺ cells was significantly higher at 24 h than at 0 h, indicating competition between hFWE1–IRES–GFP and hFWE2–IRES–RFP cells. Each co-culture combination is presented amongst the four hFWE isoforms along with IRES–GFP or IRES–RFP co-expression. Cells expressing hFWE2 or hFWE4 emerged as winners when co-cultured with cells expressing hFWE1 or hFWE3 regardless of GFP or RFP reporter. The ratio of GFP⁺ to RFP⁺ cells at 0 and 24 h for each co-culture experiment is presented quantitatively below. The ratios at 0 and 24 h for each

combination were compared statistically using a two-tailed *t*-test assuming unequal variances; $n = 4$ biologically independent experiments, *P* values shown, mean \pm s.d. **b**, Analysis of live-cell imaging is shown as heat maps to represent the total number of cells, the number of cells that died every 1.5 h, average cellular volume, and average cellular sphericity. The co-culture combinations are indicated on the left. For example, the co-culture combination of cells expressing hFWE1–IRES–GFP with cells expressing hFWE2–IRES–RFP results in the death of hFWE1–IRES–GFP cells at the expense of an increase in the number of hFWE2–IRES–RFP cells. Analysis of all co-culture combinations is presented. The data support the idea that cells expressing hFWE1 or hFWE3, when co-cultured with cells expressing hFWE2 or hFWE4, undergo cell death accompanied by loss of differentiated cellular architecture, indicated by decreased cellular volume (blue) and increased cellular sphericity (red). Each block represents a gradient scale of low (blue), medium (yellow) and high (red) for the number, size or shape of the cells ($n = 4$, analysis performed using the manual tool from Fiji and automated tools from Imaris, Genie tool used for representing data as heat maps).



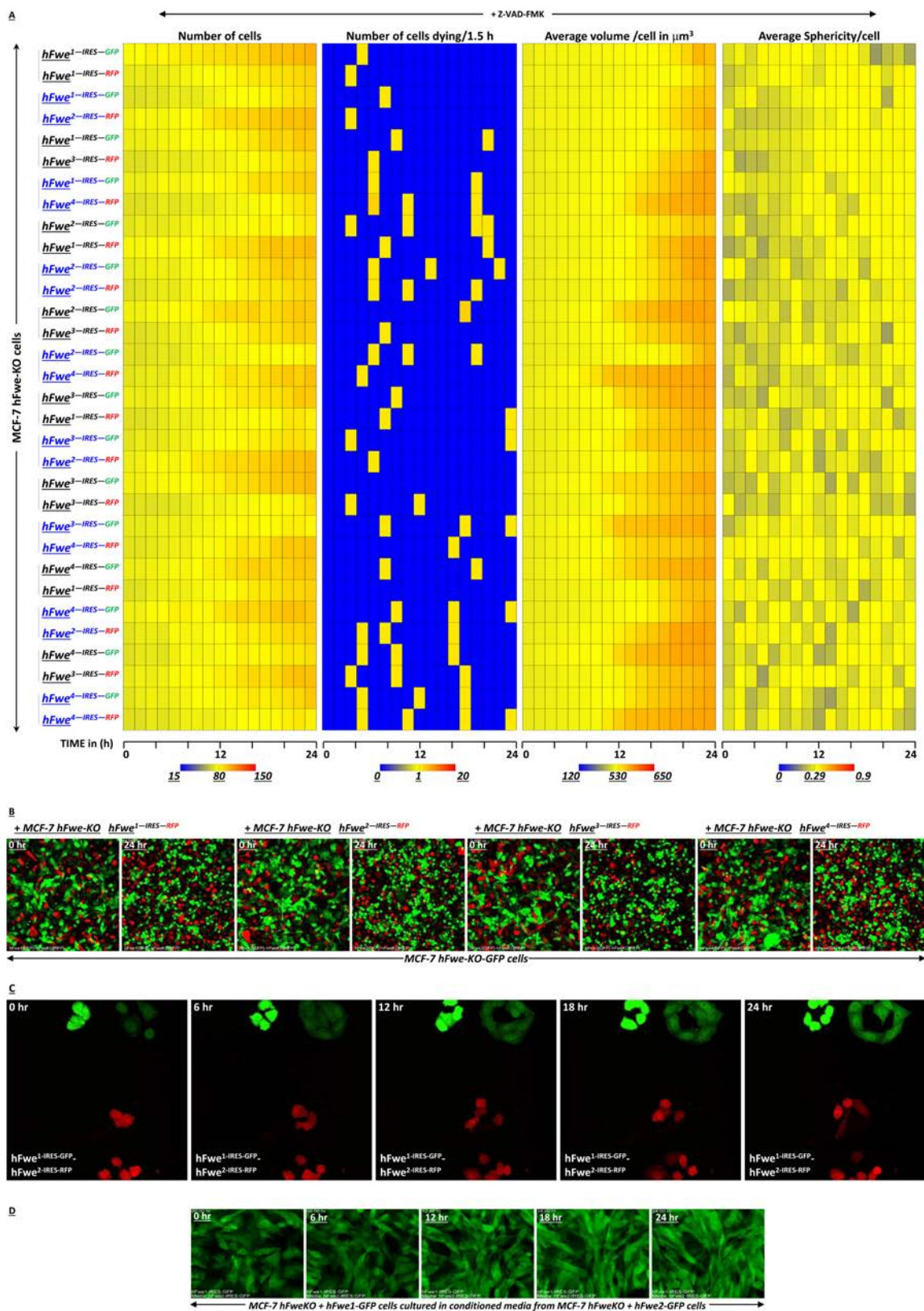
Extended Data Fig. 4 | High-resolution imaging of competition-induced Loser cell death. a, High-resolution live-cell imaging experiment (28 hr) showing cell competition in MCF-7 *hFWE*^{KO} cells expressing hFWE1-IRES-RFP and hFWE2-IRES-GFP isoforms. The co-culture results show elimination of cells carrying the Lose isoform (hFWE1-IRES-GFP); $n = 3$ biologically independent experiments with similar results. **b,** The results of live-cell imaging were confirmed using annexin-V staining and flow-cytometry-based imaging of GFP⁺ and RFP⁺ cells for each co-culture combination. Cells were sorted following 24 h of co-culture, and the percentage of apoptotic cells is displayed. The flow-based

imaging of these cells is also presented and shows no GFP⁺ signal in RFP-sorted cells or RFP⁺ signal in GFP-sorted cells. The annexin-V⁺ signal is shown in purple. For example, co-culture of cells expressing hFWE1-IRES-GFP with cells expressing hFWE2-IRES-RFP results in apoptosis of hFWE1-IRES-GFP cells, as indicated by the annexin-V⁺ signal. Together, results from live-cell imaging and flow cytometry demonstrate that cells expressing hFWE^{Lose} isoforms (hFWE1 or hFWE3) undergo apoptosis when in competition with cells expressing hFWE^{Win} isoforms (hFWE2 or hFWE4) ($n = 3$ biologically independent experiments, P values shown, two-tailed t -test, was performed for P -value calculations, mean \pm s.d.).



Extended Data Fig. 5 | Cells expressing hFWE^{LoSe} isoforms undergo caspase-dependent apoptosis during co-culture with cells expressing hFWE^{Win} isoforms. a, The effect of incubation with the pan-caspase inhibitor Z-VAD-FMK (20 μ M) on co-culture of cells expressing hFWE^{Win} or hFWE^{LoSe} isoforms. Caspase inhibition by Z-VAD-FMK rescued hFWE^{LoSe} cells expressing hFWE1 or hFWE3 from undergoing cell death induced by co-culture with hFWE^{Win} cells expressing hFWE2 or hFWE4. The ratio of GFP⁺ to RFP⁺ cells at 0 and 24 h for each co-culture experiment is presented quantitatively below. The ratios at 0 and 24 h for

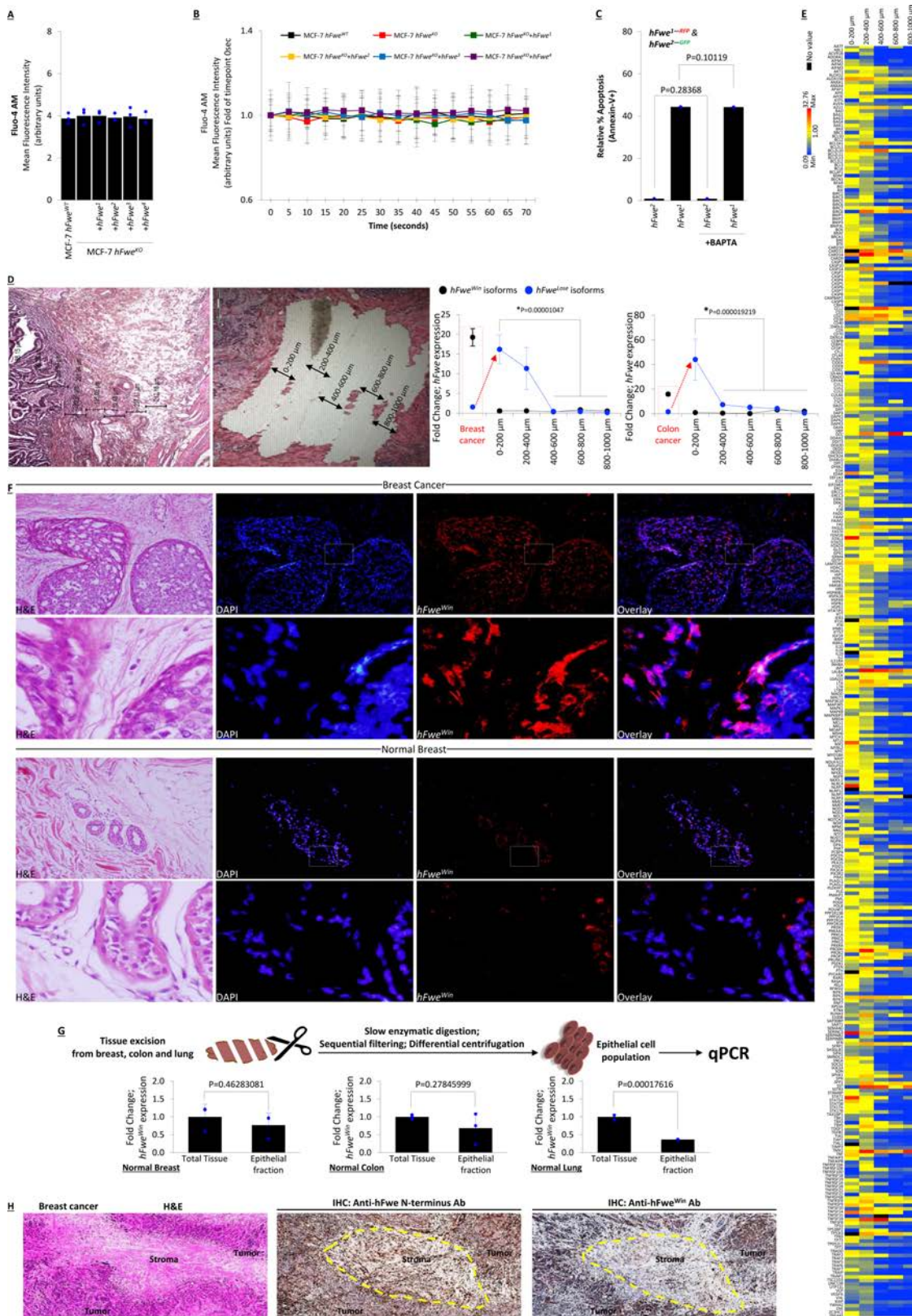
each combination were compared statistically using a two-tailed *t*-test assuming unequal variances ($n = 4$ biologically independent experiments, *P* values shown, mean \pm s.d.). **b**, Annexin-V staining and flow cytometry-based imaging of GFP⁺ and RFP⁺ cells for each co-culture combination confirms that incubation with Z-VAD-FMK prevents apoptosis in co-culture of cells expressing hFWE^{Win} or hFWE^{LoSe} isoforms ($n = 3$ biologically independent experiments, *P* values shown, two-tailed *t*-test, mean \pm s.d.).



Extended Data Fig. 6 | See next page for caption.

Extended Data Fig. 6 | Characterization of competition in co-culture assay of cells expressing hFWE^{Win} or hFWE^{Lose} isoforms. **a**, Analysis of live-cell imaging is shown as heat maps to represent the total number of cells, number of cells that died every 1.5 h, average cellular volume, and average cellular sphericity. Each block represents a gradient scale of low (blue), medium (yellow) and high (red) number, shape or size of cells. Treatment with Z-VAD-FMK blocked hFWE^{Win} cell-induced death of co-cultured hFWE^{Lose} cells, resulting in equal ratios of GFP⁺ and RFP⁺ populations ($n = 4$, analysis performed using the manual tool from Fiji and automated tools from Imaris, Genie tool used for representing data as heat maps). **b**, Imaging results show that MCF-7 *hFWE^{KO}* cells expressing each hFWE isoform independently do not outcompete co-cultured *hFWE^{KO}* cells, consistent with a mechanism of *hFWE*-mediated

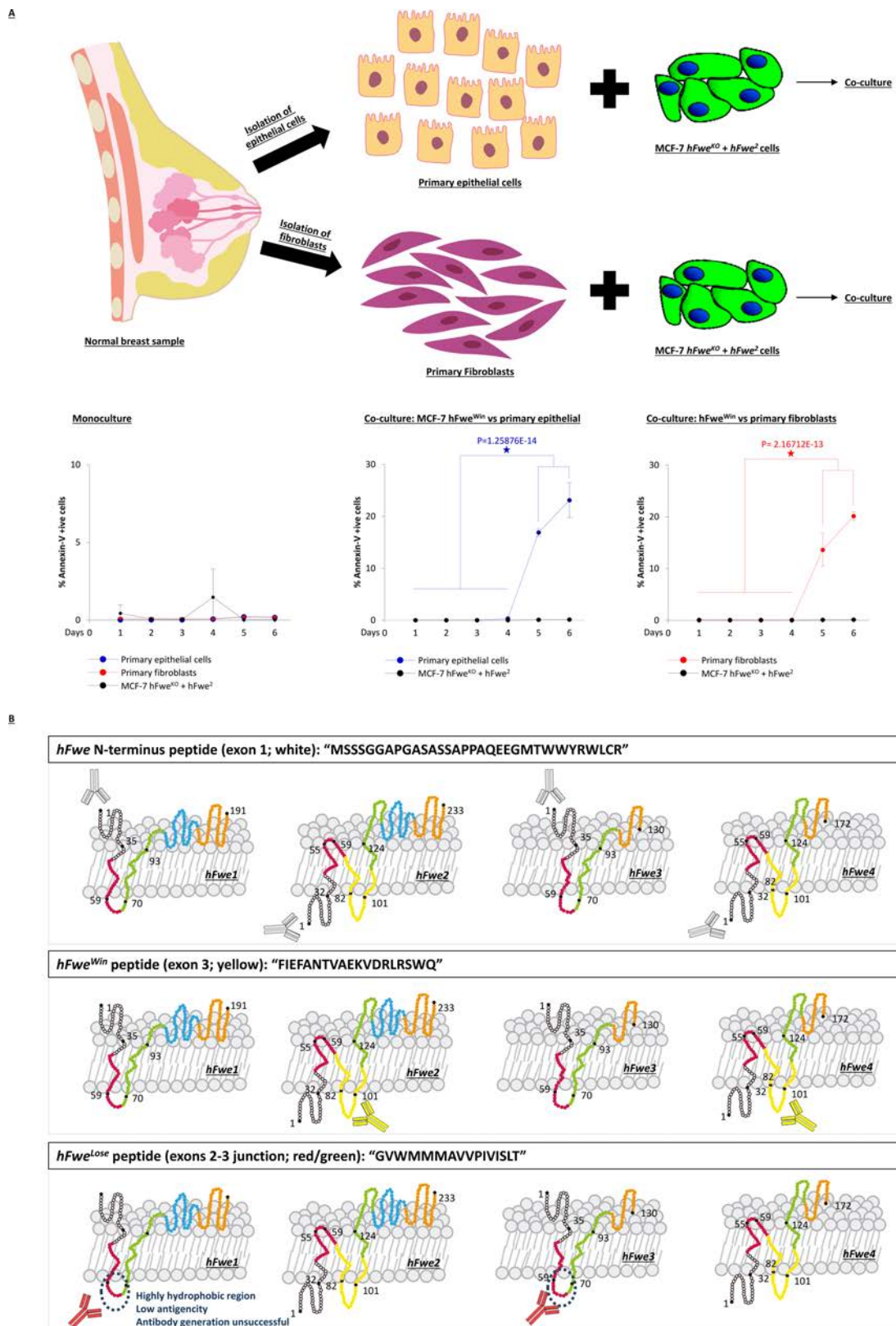
cell death supported by the presence of both hFWE^{Win} and hFWE^{Lose} isoforms ($n = 3$). **c**, Culling of cells expressing hFWE^{Lose} isoforms appeared to be contact dependent. Live-cell imaging was performed on low-density-plated MCF-7 *hFWE^{KO}* cells expressing hFWE1-IRES-GFP and hFWE2-IRES-RFP. Results show cell proliferation and absence of cell death in either cell population under conditions of low-density plating ($n = 3$ biologically independent experiments). **d**, The potential effect of secreted factors from cells expressing hFWE^{Win} isoforms was investigated. Conditioned medium from MCF-7 *hFWE^{KO}* cells expressing hFWE2-IRES-GFP did not affect viability when transferred to a culture of MCF-7 *hFWE^{KO}* cells expressing hFWE2-IRES-GFP and imaged over 24 h ($n = 3$).



Extended Data Fig. 7 | See next page for caption.

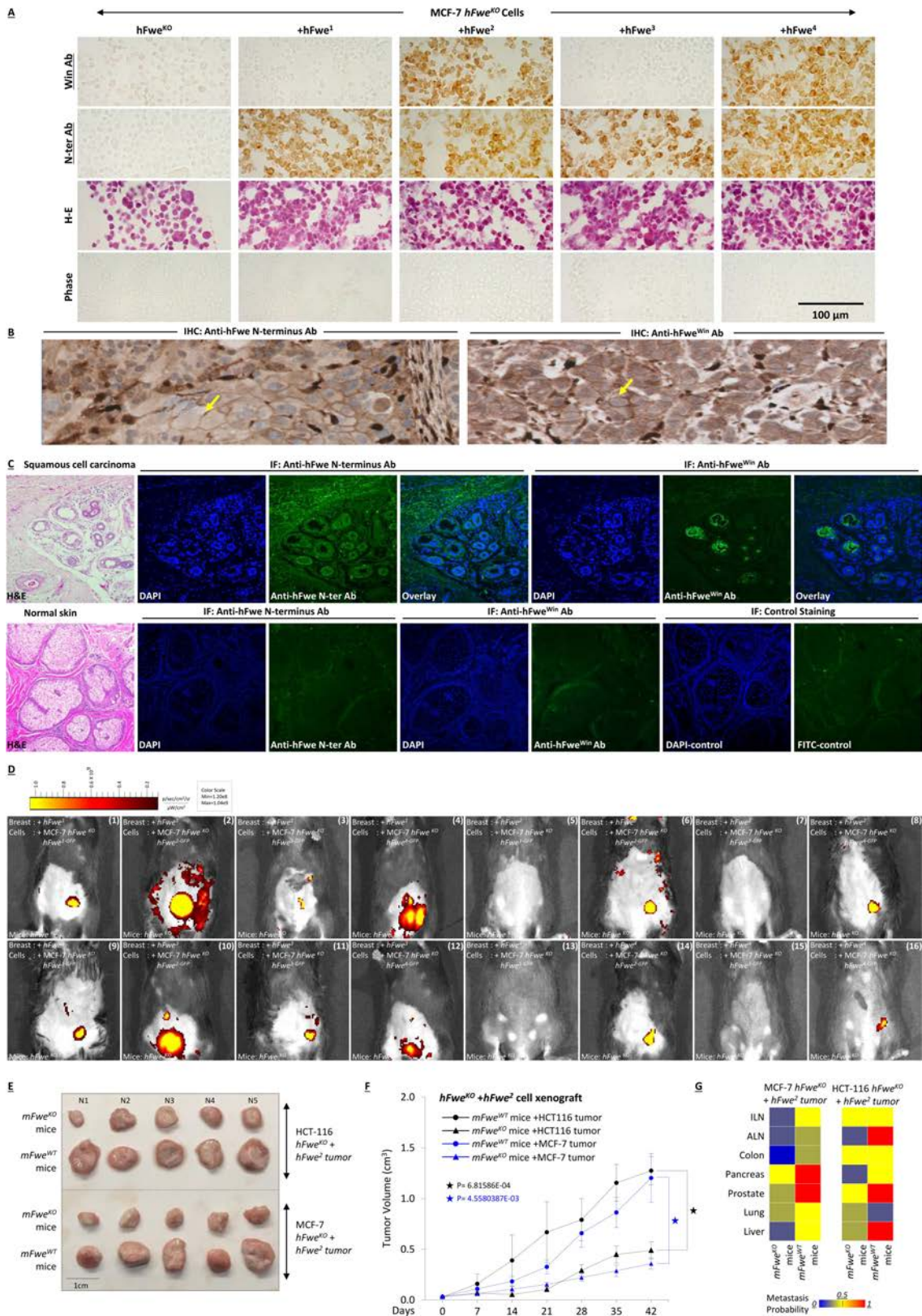
Extended Data Fig. 7 | Calcium-independent mechanism of hFWE-mediated cell competition. **a**, The potential effect of individual hFWE isoforms on intracellular calcium levels was investigated. Live-cell imaging was performed to detect levels of Fluo-4AM in MCF-7 *hFWE^{KO}* cells and MCF-7 *hFWE^{KO}* cells overexpressing single hFWE isoforms ($n = 3$ biologically independent experiments, ANOVA showed no significant differences, mean \pm s.d.). **b**, Live-cell imaging at 5-s intervals over 1 min showed constant levels of Fluo-4AM in MCF-7 *hFWE^{KO}* cells and MCF-7 *hFWE^{KO}* cells overexpressing single hFWE isoforms ($n = 3$ biologically independent experiments, ANOVA showed no significant differences, mean \pm s.d.). **c**, hFWE-mediated cell competition assay carried out in the presence or absence of the calcium chelator BAPTA-AM. Treatment with BAPTA-AM did not affect the ability of MCF-7 *hFWE^{KO}* cells expressing hFWE2 to kill co-cultured MCF-7 *hFWE^{KO}* cells expressing hFWE1 ($n = 3$ biologically independent experiments, P values shown, two-tailed t -test found no significant differences, mean \pm s.d.). **d**, Laser-capture microdissection was performed in increments of 200 μm in distance perpendicular to the defined boundary of breast tissue tumour mass. Representative images are shown for breast cancer tissue section before and after laser capture. hFWE^{Lose} isoforms were upregulated in tumour-adjacent host tissue nearest to breast cancer (0–400 μm) or colon cancer (0–200 μm). hFWE^{Win} isoforms were highly enriched within breast or colon tumour tissue but not adjacent tissue ($n = 3$ biologically independent experiments, mean \pm s.d., fold change calculated relative to the external reference of the expression of hFWE^{Win} isoforms in normal breast tissue, P values shown, two-tailed t -test). **e**, qPCR array was used to examine the expression of 354 genes involved in apoptotic pathways in samples of laser-captured tumour-adjacent host tissue. Gene expression heat map shows that host tissue in the immediate vicinity of cancer (0–400 μm) displayed upregulation of genes involved in apoptotic pathways. Host tissue farther away (400–1,000 μm) from the tumour edge displayed basal levels of apoptosis-related genes. The heat map shows

apoptotic genes that were induced (red), suppressed (blue) or unchanged (yellow) in expression. Black represents unsuccessful runs ($n = 3$). **f**, FISH shows the expression of hFWE^{Win} isoforms in FFPE samples of breast cancer tissue (top) and normal breast tissue (bottom). First column, H&E staining; second column, control DAPI staining; third column, expression of hFWE^{Win} isoforms within tumour tissue; fourth column, overlay of DAPI and hFWE^{Win} isoforms. Magnified images below each panel show expression of hFWE^{Win} isoforms specifically in tumour tissue, as these isoforms are poorly expressed in the stromal tissue surrounding the tumour and normal breast tissue ($n = 3$ for all staining). **g**, Schematic depicting the process of epithelial cell isolation from normal breast, colon, and lung tissue. Expression of the four hFWE isoforms was compared in epithelia versus total tissue by qPCR analysis ($n = 3$ biologically independent experiments, all statistically significant P values shown, two-tailed t -test, mean \pm s.d.). **h**, IHC staining of FFPE samples of breast cancer with newly developed antibodies against hFWE. Breast cancer and stromal regions are shown in the H&E images (left). The anti-hFWE^{Win} antibody is specific to Win isoforms hFWE2 and hFWE4 whereas the anti-hFWE-N-term antibody targets the common N terminus and recognizes all four isoforms. Immunohistochemistry staining shows the abundance of hFWE^{Win} isoforms within the breast cancer samples in human tumours. From this, we conclude that hFWE^{Win} proteins are expressed in the tumour but not in the stroma. To demonstrate the expression of Lose isoforms in the stroma, we compared the staining of all hFWE isoforms using our N-terminal-specific antibody with the poor expression of hFWE^{Win} in the stroma. The anti-hFWE-N-term antibody shows strong immunoreactivity and equal distribution of staining in the tumour and stromal tissue. We find no positive signal for hFWE^{Win} isoforms in the stroma, but we find strong expression of total hFWE (hFWE^{Win} and hFWE^{Lose} combined) in the stroma near the tumour. From this, we can conclude that Lose isoforms are expressed in the stroma. This experiment was repeated independently three times with similar results.



Extended Data Fig. 8 | Dynamics of hFWE-mediated cell competition between cancer and normal cells. a, Protocol for observing hFWE-mediated cell competition between hFWE^{Win}-expressing cancer cells and primary cultures of human epithelial cells and fibroblasts. MCF-7 hFWE^{KO} cells overexpressing hFWE^{Win} isoforms outcompeted and induced apoptosis of co-cultured primary breast normal epithelial cells or fibroblasts over 6 days ($n = 3$ biologically independent experiments, all statistically significant P values are shown, ANOVA, mean \pm s.d.). **b,** hFWE^{Win} isoforms (hFWE2 and hFWE4) and hFWE^{Lose} isoforms

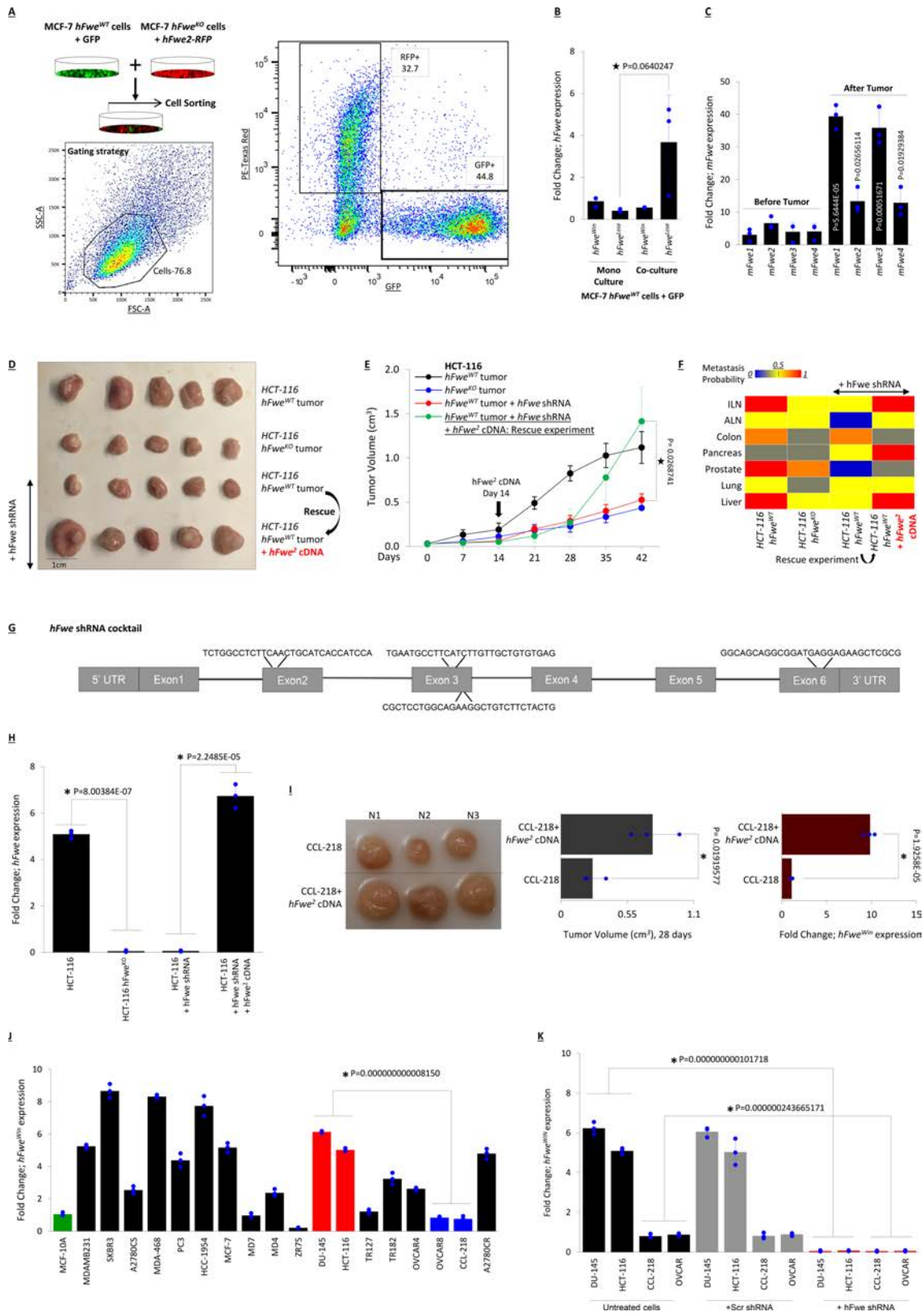
(hFWE1 and hFWE3) are characterized by intra-exonic inclusions. The in silico model shows predicted transmembrane structures of the four hFWE proteins. An antibody was raised against the common N terminus (exon 1), which is included in all four isoforms. Another antibody was raised to specifically recognize the hFWE^{Win} isoforms (which share exon 3). Owing to the similarity in sequences to hFWE^{Win} isoforms and low antigenicity of the peptide sequence at the junction of exons 2 and 4, generation of an antibody specific to hFWE^{Lose} isoforms was not possible.



Extended Data Fig. 9 | See next page for caption.

Extended Data Fig. 9 | Generation of antibodies against hFWE^{Win} isoforms (hFWE2 and hFWE4) or the common hFWE N terminus and expression in human cancers. **a**, Immunocytochemistry of hFWE isoforms in paraffin-embedded and sectioned human MCF-7 cells using novel anti-hFWE antibodies. The specificity was validated by immunocytochemistry of MCF-7 *hFWE^{KO}* cells with or without overexpression of individual hFWE isoforms. Cells were stained with anti-hFWE-N-term antibody or anti-hFWE^{Win} antibody. Immunocytochemistry results confirm antibody specificity in paraffin sections with MCF-7 *hFWE^{KO}* cells with or without overexpression of individual hFWE isoforms. The anti-hFWE^{Win} antibody does not stain sections with *hFWE^{KO}* cells, and recognizes specifically hFWE2 and hFWE4, but not the hFWE^{Lose} isoforms hFWE1 and hFWE3 (row 1). The anti-hFWE-N-term antibody is also negative for staining in control *hFWE^{KO}* cells but detected positive membrane staining for each of the four hFWE isoforms (row 2; $n = 3$). **b**, Immunohistochemistry of hFWE proteins in sections from clinical breast cancer samples ($n = 3$). Arrows indicate membrane staining. **c**, Immunofluorescence staining of hFWE proteins in human SCC tissue shows an abundance of hFWE^{Win} isoforms within defined cancer lesions, whereas the anti-hFWE-N-term antibody stained both stroma and cancer tissue (top; $n = 3$) when compared with normal skin (bottom; $n = 3$). **d**, Tumour volumes were measured and analysed for each of the 16 combinations of hFWEX-IRES-GFP expression in MCF-7 *hFWE^{KO}* xenografted cells and hFWE

isoform expression within *Fwe^{KO}* mouse mammary tissue ($n = 3$). In vivo bioluminescence imaging (using the IVIS system) was used to detect and measure the fluorescence of GFP⁺ cancer cells in tumours resulting from all genetic combinations at 28 days post-implantation. Substantially reduced tumour growth was observed when mammary tissue expressed hFWE^{Win} isoforms and cancer cells expressed hFWE^{Lose} isoforms. By contrast, tumour growth is strongly promoted when mammary tissue expresses hFWE^{Lose} isoforms and cancer cells express hFWE^{Win} isoforms ($n = 3$). **e**, Tumorigenic potential of HCT-116 (colon origin) or MCF-7 (breast origin) *hFWE^{KO}* cells overexpressing hFWE2 in recipient *Fwe^{WT}* and *Fwe^{KO}* mice. Tumour growth of both *Fwe^{KO}* breast and colon cancer cell lines overexpressing the Win isoform hFWE2 was greater in *Fwe^{WT}* mice than in *Fwe^{KO}* mice. Photos of resected tumours are shown. **f**, Tumour volumes were measured every week over 42 days for groups shown in **a**. *hFWE^{KO}* colon- or breast-derived tumours overexpressing hFWE2 showed significantly higher growth in *Fwe^{WT}* mice than in *Fwe^{KO}* mice ($n = 5$, P values shown, one-tailed t -test, mean \pm s.d.). **g**, At the conclusion of tumour growth experiments, mice were examined for the presence or absence of metastases in inguinal lymph nodes (ILN), axillary lymph nodes (ALN), colon, pancreas, prostate, lung, and liver. Heat map scale indicates the probability of metastasis. Results show a marked reduction in the metastatic potential of both breast and colon cancer *hFWE^{KO}* cells overexpressing hFWE2 when xenografted into *Fwe^{KO}* mice as compared to *Fwe^{WT}* mice ($n = 5$ each group).



Extended Data Fig. 10 | See next page for caption.

Extended Data Fig. 10 | Endogenous hFWE in human cancer cell lines and tumorigenic potential.

a, Culture experiments were conducted to examine the dynamics of hFWE^{Win} and hFWE^{Lose} isoform expression. MCF-7 *hFWE*^{KO} cells expressing hFWE2-RFP were co-cultured with wild-type MCF-7 cells expressing GFP for 24 h and sorted for analysis of hFWE isoform expression. *n* = 3 biologically independent experiments with similar results. **b**, Co-culture of MCF-7 *hFWE*^{KO} cells expressing hFWE2-RFP with wild-type MCF-7 cells expressing GFP caused upregulation of hFWE^{Lose} isoforms in wild-type MCF-7 cells. qPCR analysis of the expression of hFWE^{Win} and hFWE^{Lose} isoforms in GFP⁺ wild-type MCF-7 cells sorted from co-culture shows a significant increase in hFWE^{Lose} isoforms (bar 4) when compared with monocultured wild-type MCF-7 cells (bar 2). *n* = 3 biologically independent experiments with similar results; fold change calculated relative to the expression of hFWE^{Win} isoforms in monocultured GFP⁺ wild-type MCF-7 cells, all statistically significant *P* values shown, two-tailed *t*-test, mean ± s.d. **c**, MCF-7 cells expressing hFWE2 were xenografted into *Fwe*^{WT} mice to assess their tumorigenic potential and the host expression of endogenous hFWE isoforms compared to control. The mouse tissue adjacent to the tumour showed a significant increase in expression of hFWE^{Lose} isoforms at 21 days post-xenograft. *n* = 3 biologically independent experiments with similar results; all statistically significant *P* values shown, one-tailed *t*-test, mean ± s.d. **d**, The effect of anti-*hFWE* shRNA cocktail on the tumorigenic potential of HCT-116 cells. Row 1, growth potential of HCT-116 *hFWE*^{WT} cells. Row 2, knockout of *hFWE* in these cells significantly reduced tumour growth. Row 3, treatment of HCT-116 *hFWE*^{WT} cells with anti-*hFWE* shRNA reduced tumour volume. Row 4, Rescue experiment in which similar *hFWE* shRNA-treated tumours to row 3 were infected with lentivirus overexpressing hFWE2 14 days after implantation. These tumours are significantly larger than those in row 3. **e**, Tumour volumes for experiments shown in Fig. 4a were measured weekly, and growth patterns were analysed over 42 days for groups shown in **a**. Growth curves show the reduced growth of tumours from HCT-116 *hFWE*^{KO} cells (blue) and *hFWE* shRNA-treated HCT-116 *hFWE*^{WT} cells (red). Green line shows rescue experiment and growth pattern changes in *hFWE* shRNA-treated

HCT-116 *hFWE*^{WT} tumours expressing with hFWE2 (*n* = 5, *P* values shown, one-tailed *t*-test, mean ± s.d.). **f**, All mice used in the study were examined for the presence or absence of metastases in ILN, ALN, colon, pancreas, prostate, lung and liver. Heat map scale indicates the probability of metastasis. Metastatic potential was reduced by knockout or knockdown of *hFWE* in HCT-116 cells (compare column 1 with columns 2 and 3). The rescue of tumour growth by re-introduction of *hFWE2* cDNA was accompanied by an increase in metastasis of these cells (compare column 3 with column 4; *n* = 5 each group). **g**, A cocktail of shRNAs were designed to knock down all four isoforms of hFWE. All shRNAs were checked for off-target effects. **h**, Gene expression analysis confirmed deletion of total *hFWE* in HCT-116 *hFWE*^{KO} cells. Exogenous expression of *hFWE2* cDNA was detectable as the total *hFWE* expression in wild-type HCT-116 cells co-treated with anti-*hFWE* shRNA (observed in resected tumours). *n* = 3 biologically independent experiments, fold change calculated relative to expression of hFWE^{Win} isoforms in MCF-10A cells, *P* values shown, two-tailed *t*-test, mean ± s.d. **i**, Tumorigenic potential of wild-type CCL-218 cells and CCL-218 cells overexpressing hFWE2. Xenografts overexpressing *hFWE2* cDNA showed increased tumour volume at 28 days. Photos of resected tumours are shown. *n* = 3 biologically independent experiments with similar results, all statistically significant *P* values shown, ANOVA, mean ± s.d. Control qPCR experiment demonstrates the overexpression of *hFWE2* in CCL-218 tumours at day 28. *n* = 3 biologically independent experiments, fold change calculated relative to expression of hFWE^{Win} isoforms in MCF-10A cells, *P* values shown, two-tailed *t*-test, mean ± s.d. **j**, Endogenous expression of the four hFWE isoforms in 19 cancer cell lines of multiple origins (*n* = 3 biologically independent experiments, fold change is calculated relative to expression of hFWE^{Win} isoforms in MCF-10A cells, *P* values shown, ANOVA, mean ± s.d.). **k**, Gene expression analysis shows efficient shRNA-mediated knockdown of total *hFWE* in HCT-116, DU-145, CCL-218 and OVCAR-8 tumours (observed in resected tumours). *n* = 3 biologically independent experiments, fold change calculated relative to expression of hFWE^{Win} isoforms in MCF-10A cells, *P* values shown, ANOVA, mean ± s.d.

Reporting Summary

Nature Research wishes to improve the reproducibility of the work that we publish. This form provides structure for consistency and transparency in reporting. For further information on Nature Research policies, see [Authors & Referees](#) and the [Editorial Policy Checklist](#).

Statistics

For all statistical analyses, confirm that the following items are present in the figure legend, table legend, main text, or Methods section.

- | | |
|-----|-----------|
| n/a | Confirmed |
|-----|-----------|
- The exact sample size (n) for each experimental group/condition, given as a discrete number and unit of measurement
 - A statement on whether measurements were taken from distinct samples or whether the same sample was measured repeatedly
 - The statistical test(s) used AND whether they are one- or two-sided
Only common tests should be described solely by name; describe more complex techniques in the Methods section.
 - A description of all covariates tested
 - A description of any assumptions or corrections, such as tests of normality and adjustment for multiple comparisons
 - A full description of the statistical parameters including central tendency (e.g. means) or other basic estimates (e.g. regression coefficient) AND variation (e.g. standard deviation) or associated estimates of uncertainty (e.g. confidence intervals)
 - For null hypothesis testing, the test statistic (e.g. F , t , r) with confidence intervals, effect sizes, degrees of freedom and P value noted
Give P values as exact values whenever suitable.
 - For Bayesian analysis, information on the choice of priors and Markov chain Monte Carlo settings
 - For hierarchical and complex designs, identification of the appropriate level for tests and full reporting of outcomes
 - Estimates of effect sizes (e.g. Cohen's d , Pearson's r), indicating how they were calculated

Our web collection on [statistics for biologists](#) contains articles on many of the points above.

Software and code

Policy information about [availability of computer code](#)

Data collection

Zen2.3 SP1, CFX manager, Step1 softwarev2.3, Amnis ImageStream MK II Imaging, Becton Dickinson FACS ARIA Fusion, Becton Dickinson FACS ARIA IIIu, Becton Dickinson-LSRII H274, MACSQuant Analyzer, Palm Robo Software, IVIS 200 Vivo Vision System (Xenogen), Philip Ultra Fast Scanner 1.6, Leica TCS SP8 confocal laser microscope, Nikon A1 HD25 confocal microscope, Zeiss LSM-800 with Airy Scan Confocal Microscope, BZ-X700 microscope, Leica Cryostat 3050S, Leica Microsystems, Zeiss Palm MicroBeam IV Laser Capture Microdissection system, PredictProtein 2013.

Data analysis

Flow-Jo.V9, Flow-Jo.V10, BD FACS DIVA, Inspire Imaris, Fiji, IVIS 200 Vivo Vision System (Xenogen), CFX manager, Step1 softwarev2.3. Microsoft excel was used to calculate mean, standard deviation, and p value.

For manuscripts utilizing custom algorithms or software that are central to the research but not yet described in published literature, software must be made available to editors/reviewers. We strongly encourage code deposition in a community repository (e.g. GitHub). See the Nature Research [guidelines for submitting code & software](#) for further information.

Data

Policy information about [availability of data](#)

All manuscripts must include a [data availability statement](#). This statement should provide the following information, where applicable:

- Accession codes, unique identifiers, or web links for publicly available datasets
- A list of figures that have associated raw data
- A description of any restrictions on data availability

Source data for Figures 2-4 and Extended Data Figures 1-8, 10 are provided with the paper.

Field-specific reporting

Please select the one below that is the best fit for your research. If you are not sure, read the appropriate sections before making your selection.

- Life sciences Behavioural & social sciences Ecological, evolutionary & environmental sciences

For a reference copy of the document with all sections, see [nature.com/documents/nr-reporting-summary-flat.pdf](https://www.nature.com/documents/nr-reporting-summary-flat.pdf)

Life sciences study design

All studies must disclose on these points even when the disclosure is negative.

Sample size	Power analysis (what method of power analysis) was used as method to determine sample size where ever was appropriate.
Data exclusions	No data was excluded from analysis.
Replication	All experiments were repeated minimum with 3 replicates with reproducible results. No replicates were excluded.
Randomization	All mice were randomly allocated to the experimental groups
Blinding	Investigators were blinded during data collection and analysis for the following experiments: 1. Gene expression analysis of Fwe using RNA collected from laser-capture microdissected FFPE human cancer samples, and qPCR apoptosis gene microarray (Fig 2 A-C).

Reporting for specific materials, systems and methods

We require information from authors about some types of materials, experimental systems and methods used in many studies. Here, indicate whether each material, system or method listed is relevant to your study. If you are not sure if a list item applies to your research, read the appropriate section before selecting a response.

Materials & experimental systems

n/a	Involvement in the study
<input type="checkbox"/>	<input checked="" type="checkbox"/> Antibodies
<input type="checkbox"/>	<input checked="" type="checkbox"/> Eukaryotic cell lines
<input checked="" type="checkbox"/>	<input type="checkbox"/> Palaeontology
<input type="checkbox"/>	<input checked="" type="checkbox"/> Animals and other organisms
<input checked="" type="checkbox"/>	<input type="checkbox"/> Human research participants
<input checked="" type="checkbox"/>	<input type="checkbox"/> Clinical data

Methods

n/a	Involvement in the study
<input checked="" type="checkbox"/>	<input type="checkbox"/> ChIP-seq
<input type="checkbox"/>	<input checked="" type="checkbox"/> Flow cytometry
<input checked="" type="checkbox"/>	<input type="checkbox"/> MRI-based neuroimaging

Antibodies

Antibodies used	2 Anti-Flower Primary Antibodies; a) Anti-Win Ab; Dilution: 1:500 and b) Anti-N-ter Ab; Dilution: 1:500 Secondary Ab used for tissue immunohistochemistry: Goat Anti-Mouse IgG HRP-conjugated (Thermo Fisher Sci); Dilution: 1:2000 Secondary Ab used for tissue immunofluorescence and immunocytochemistry: Goat Anti-Mouse IgG Alexa Fluor 488 (Thermo Fisher Sci); Dilution: 1:1000
Validation	The antibodies were custom synthesized in partnership with Genscript, USA. All the antibodies were authenticated and validated as part of custom order by Genscript. We have also validated the specificity of our antibodies and presented data in manuscript in the following immunocytochemistry experiments: 1. Anti-Fwe-Win Antibody: Positive signal observed in MCF-7 hFwe KO cells+hFwe-Win isoforms and negative signal in MCF-7 hFwe KO cells and MCF-7 hFwe KO cells+hFwe-Lose isoforms. 2. Anti-N-ter Antibody: Positive signal observed in MCF-7 hFwe KO cells+hFwe-Win/Lose isoforms and no signal detected in MCF-7 hFwe KO cells.

Eukaryotic cell lines

Policy information about [cell lines](#)

Cell line source(s)	The following cell lines included in this study were obtained from ATCC: A2780-CR, A2780-CS, CCL-218, DU-145, HCC-1954, HCT-116, MCF-7, MCF 10A, MD-4, MD-7, MDA-MB-231, MDA-MB-468, PC-3, SK-BR-3, TR-127, TR-182, ZR-75. HEK293 were obtained from Cell Biolabs, Inc. OVCAR-4, OVCAR-8 were kindly provided by Selvendiran Karuppaiyah, Ohio State University. Normal epithelial cells and fibroblasts isolated from normal breast tissue were kindly provided by Harikrishna Nakshatri,
---------------------	--

Komen Tissue Bank, Indiana University Purdue University Indianapolis.

Authentication

All cell lines were authenticated or received with certificates for authentication.

Mycoplasma contamination

All cells were tested and were certified as negative for mycoplasma contamination.

Commonly misidentified lines
(See [ICLAC](#) register)

No commonly misidentified cell lines as per ICLAC were included in this study.

Animals and other organisms

Policy information about [studies involving animals](#); [ARRIVE guidelines](#) recommended for reporting animal research

Laboratory animals

Female and male Swiss nude mice age 4-6 weeks; female Fwe-Knockout and Fwe-Wildtype C57BL/6 mice age 4-6 weeks were used in this study.

Wild animals

No wild animals were included in this study.

Field-collected samples

No field-collected samples were included in this study.

Ethics oversight

All animal work was approved by Institutional Animal Care and Use Committee (IACUC) affiliated with Dartmouth College and Institutional Animal Ethics Committee at Champalimaud Foundation.

Note that full information on the approval of the study protocol must also be provided in the manuscript.

Flow Cytometry

Plots

Confirm that:

- The axis labels state the marker and fluorochrome used (e.g. CD4-FITC).
- The axis scales are clearly visible. Include numbers along axes only for bottom left plot of group (a 'group' is an analysis of identical markers).
- All plots are contour plots with outliers or pseudocolor plots.
- A numerical value for number of cells or percentage (with statistics) is provided.

Methodology

Sample preparation

All samples were prepared as described in the Methods section.

Instrument

Amnis ImageStream MK II Imaging, Becton Dickinson FACS ARIA Fusion, Becton Dickinson FACS ARIA IIIu, Becton Dickinson-LSRII H274, MACSQuant Analyzer, LSR Fortessa X20, BD FACS Aria Fusion, BD FACS ARIA III

Software

FlowJo.V9, FlowJo.V10

Cell population abundance

High purity sorted samples were used in the study.

Gating strategy

All preliminary FSC/SCC gates to remove debris and other events of the starting cell population and boundaries between positive and negative staining cell populations are defined. Gating strategies are explained in detail in the legends and methods sections. Fig ED10D presents a figure exemplifying the gating strategy.

- Tick this box to confirm that a figure exemplifying the gating strategy is provided in the Supplementary Information.